รายงานวิจัยฉบับสมบูรณ์

โครงการ Effects of Geometry, Alignment, Grain Size, Strain Rate, and Tribology on Curving Tendency of Micro-Extruded Pins by Using Finite Element Simulation

โดย ผศ.ดร.นำพล มหายศนันท์ และคณะ

กรกฎาคม 2563

สัญญาเลขที่ MRG5980148

รายงานวิจัยฉบับสมบูรณ์

โครงการ Effects of Geometry, Alignment, Grain Size, Strain Rate, and Tribology on Curving Tendency of Micro-Extruded Pins by Using Finite Element Simulation

ผู้วิจัย สังกัด
ผศ.ดร.นำพล มหายศนันท์ มหาวิทยาลัยขอนแก่น

สนับสนุนโดยสำนักงานคณะกรรมการการอุดมศึกษาและสำนักงานกองทุนสนับสนุนการวิจัย

(ความเห็นในรายงานนี้เป็นของผู้วิจัย สกอ. และ สกว. ไม่จำเป็นต้องเห็นด้วยเสมอไป)

บทคัดย่อ

รหัสโครงการ: MRG5980148

ชื่อโครงการ: Effects of Geometry, Alignment, Grain Size, Strain Rate, and Tribology on Curving Tendency of Micro-Extruded Pins by Using Finite Element Simulation

ชื่อนักวิจัย และสถาบัน: ผศ.ดร.นำพล มหายศนันท์

อีเมล์: numpon@kku.ac.th

ระยะเวลาโครงการ: 1 พฤษภาคม 2559 ถึง 2 พฤษภาคม 2561 (2 ปี)

บทคัดย่อ: การเพิ่มมูลค่าให้กับผลิตภัณฑ์อะลูมิเนียมที่ผลิตในประเทศไทยนั้นจำเป็นที่ต้องพัฒนาผลิตภัณฑ์ที่จะสามารถตอบโจทย์ความต้องการประยุกต์ใชผลิตภัณฑ์ในรูปแบบใหม่ กระบวนการอัดรีดขึ้นรูปขนาดไมโคร (Micro-Extrusion) เป็นหนึ่งในเทคโนโลยีที่มีความเป็นไปได้สูงที่จะช่วยผลักดันให้เกิดผลิตภัณฑ์อะลูมิเนียมมูลค่าสูงได้ อย่างไรก็ตาม Micro-Extrusion นั้นถือว่าเป็นเทคโนโลยีที่พึ่งมีการถูกพัฒนาขึ้นเมื่อไม่นานมานี้สำหรับการขึ้นรูปชิ้นส่วนขนาดเล็กระดับไมโคร จึงทำให้ความรู้ความเข้าใจพื้นฐานทางด้านพฤติกรรมการเสียรูปและแรงเสียดทานนั้นยังไม่เป็นที่เข้าใจอย่างถ่องแท้ ซึ่งส่งผลทำให้เกิดการเสียรูปของชิ้นงานในรูปแบบที่ไม่ได้ตามความคาดหวัง ดังนั้นโครงการนี้ได้ศึกษาเกี่ยวกับปัจจัยหลักที่ส่งผลกระทบกับแนวโน้มการเสียรูปแบบโค้งของชิ้นงานอัดรีดขึ้นรูปอะลูมิเนียมเกรด 6063 ระดับไมโคร โดยมีตัวแปรหลัก คือ รูปทรงและการวางแนวของแม่พิมพ์ ขนาดเกรนและการวางตัวของเกรน และไทรโบโลยี ซึ่งศึกษาโดยการใช้การจำลองทางไฟไนต์เอลิเมนต์ที่ได้สอบทวนกับการทดสอบจริงด้วยเครื่องอัดรีดขึ้นรูประดับไมโคร ผลการจำลองนั้นได้อธิบายถึงปัจจัยหลักที่ส่งผลกับการเสียรูปแบบโค้ง ความสัมพันธ์ของตัวแปรหลักกับการเสียรูปแบบโค้งได้มีการพัฒนาขึ้น นอกจากนี้แล้วผลกระทบต่อการใช้พลังงานในกระบวนการอัดรีดขึ้นรูประดับไมโครจากปัจจัยที่พิจารณานั้นยังได้มีการศึกษาอีกด้วย จากผลการวิเคราะห์ความสัมพันธ์ที่เกิดขึ้นทำให้นำมาเป็นองค์ความรู้เกี่ยวกับการเกิดขึ้นของการเสียรูปแบบโค้งได้ ซึ่งผลที่ได้รับจากโครงการนี้จะสามารถนำไปถ่ายทอดให้กับผู้ประกอบการอัดรีดขึ้นรูปอะลูมิเนียมของประเทศไทยในด้านการออกแบบ การเลือกแม่พิมพ์ วัสดุ และพารามิเตอร์ของกระบวนการอัดรีดขึ้นรูปที่เหมาะสม และผลลัพธ์ที่ได้จากโครงการนี้จะสามารถนำไปต่อยอดเพื่อให้เป็นหนึ่งในแรงขับเคลื่อนหลักสำหรับอุตสาหกรรมการผลิตอะลูมิเนียมของประเทศไทยเพื่อให้มีความสามารถในการแข่งขันสูงขึ้นในตลาด

คำหลัก: aluminum alloy; curvature; grain size; micro-extrusion; finite element analysis; tribology

Abstract

Project Code: MRG5980148

Project Title: Effects of Geometry, Alignment, Grain Size, Strain Rate, and Tribology on Curving Tendency of Micro-Extruded Pins by Using Finite Element Simulation

Investigator: Asst.Prof.Dr. Numpon Mahayotsanun

E-mail Address: numpon@kku.ac.th

Project Period: May 1, 2017 to May 2, 2019 (2 Years)

Abstract: In order to add value to aluminum extrusion products manufactured by Thai companies, it is necessary to develop high-quality products that meet the requirements of the emerging applications. The micro-extrusion process is one of the promising technologies enabling Thai aluminum extrusion companies to respond to such demand. Since micro-extrusion is considered a recent technology dealing with miniaturized parts, there still lacks a fundamental understanding of deformation and tribological behaviors, mainly when undesirable extruded shapes appear. This project investigated the major factors influencing the curving tendency of micro pins formed by using micro-extrusion of aluminum alloy 6063. The considered factors were: (1) tool geometry and alignment, (2) billet grain size and orientation, and (3) tribology. The finite element simulations were carried out to investigate these factors, and the simulation results were validated with those of the micro-extrusion experiments. The driving mechanisms and effects of each considered factor to the curving tendency of micro-extruded pins were explained. The relationships among these factors affecting the curving tendency were developed. In addition, the influences of the considered factors to the energy consumption in the micro-extrusion process were also examined. Based on the acquired knowledge and relationships, the curving tendency of micro-extruded pins could be predicted. The analysis obtained from this study would be valuable to the Thai aluminum extrusion industry in terms of design, selection, and optimization of tools, materials, and process parameters in micro-extrusion. Most importantly, this project's outcome will be a driving force for the Thai aluminum extrusion industry to be competitive in the emerging markets.

Keywords : aluminum alloy; curvature; grain size; micro-extrusion; finite element analysis; tribology

Executive Summary

โครงการวิจัยนี้ศึกษาผลกระทบของ รูปทรงและการวางแนวของแม่พิมพ์ ขนาดเกรนและการเรียงตัวของเกรน และไทรโบโลยี ต่อแนวโน้มการเสียรูปแบบโค้ง และพลังงานที่ใช้ในกระบวนการอัดรีดขึ้นรูปอะลูมิเนียม 6063 ในระดับไมโครโดยการใช้การจำลองทางไฟไนต์เอลิเมนต์ โดยจากผลการจำลองนั้น ตัวแปรหลักที่ส่งผลต่อการเสียรูปแบบโค้ง คือ Die Shift (DS) Bearing Length (LB) และ Grain Size and Grain Orientation เมื่อขนาดของเกรนมีขนาดใหญ่ (จำนวนเกรนประมาณ 1-2 เกรนต่อแนวขวางของชิ้นงาน) และเมื่อเพิ่มค่าของตัวแปรเหล่านี้จะทำให้พลังงานที่ใช้ในกระบวนการอัดรีดขึ้นรูปสูงขึ้น Extrusion Ratio (ER) Die Angle (α) Billet Length (BL) Bearing Length (LB) และ Coefficient of Friction (COF) โดยผลที่ได้จากงานวิจัยในโครงการนี้จะนำไปใช้ต่อยอดในการออกแบบและควบคุมขนาดของเกรน การเรียงตัวของเกรน เพื่อควบคุมความโค้งของชิ้นงานในระดับไมโครให้ได้ตามที่ต้องการโดยไม่เกิดการสูญเสีย

1. Objectives

วัตถุประสงค์หลักของโครงการวิจัยมีดังต่อไปนี้

1.1 ศึกษาผลกระทบของ รูปทรงและการวางแนวของแม่พิมพ์ ขนาดเกรนและการเรียงตัวของเกรน และไทรโบโลยี ต่อแนวโน้มการเสียรูปแบบโค้งของกระบวนการอัดรีดขึ้นรูปอะลูมิเนียม 6063 ในระดับไมโครโดยการใช้การจำลองทางไฟไนต์เอลิเมนต์

1.2 ศึกษาผลกระทบของรูปร่างของแม่พิมพ์ การวางแนวของแม่พิมพ์ และไทรโบโลยีกับการใช้พลังงานในกระบวนการอัดรีดขึ้นรูปอะลูมิเนียมในระดับไมโครโดยการใช้การจำลองทางไฟไนต์เอลิเมนต์

2. Materials and Methods

2.1 Micro-Extrusion Process

กระบวนการ Micro-Extrusion นั้นเป็นกระบวนการอัดรีดขึ้นรูปซึ่งเป็นการอัดวัสดุผ่านแม่พิมพ์แล้วเปลี่ยนรูปร่างวัสดุให้มีการเสียรูปแบบพลาสติกให้มีขนาดและรูปทรงที่มีพื้นที่หน้าตัดเล็กลงตามดังแสดงในรูปที่ 1 และมีเครื่องทดสอบสำหรับการอัดรีดขึ้นรูประดับไมโคร (Micro-Extrusion Machine) นั้นแสดงในรูปที่ 2

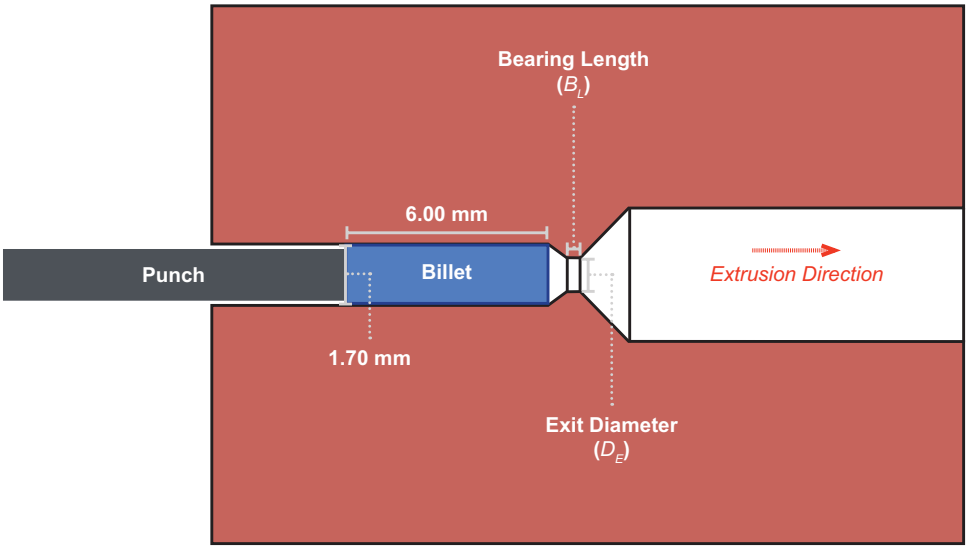

รูปที่ 1 Micro-extrusion process

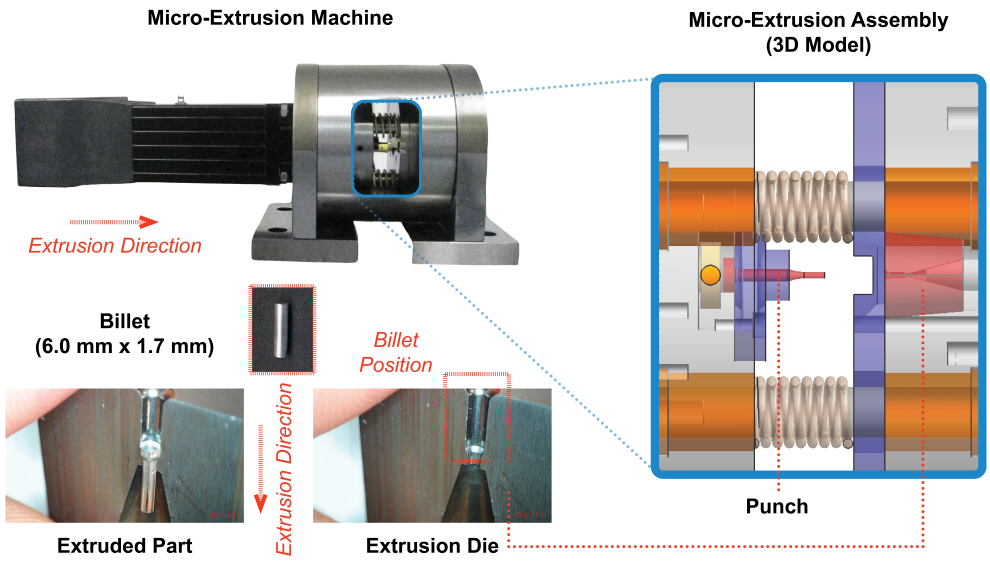

รูปที่ 2 Micro-extrusion machine

2.2 Materials

วัสดุที่ใช้ในการทดสอบ คือ อะลูมิเนียมเกรด 6063 ที่มีเส้นผ่านศูนย์กลาง 1.7 mm ยาว 6.0 mm และวัสดุที่ใช้ในการทำแม่พิมพ์ คือ SKD11 (รายละเอียดอยู่ในภาคผนวก)

2.3 Finite Element (FE) Simulation

การจำลองทางไฟไนต์เอลิเมนต์นั้นได้นำมาใช้ในการศึกษาปัจจัยที่สำคัญที่ส่งผลกระทบต่อการเสียรูปแบบโค้งของชิ้นงานอัดรีดขึ้นรูปอะลูมิเนียมดังแสดงในรูปที่ 3 (รายละเอียดอยู่ในภาคผนวก) โดยความเร็วที่ใช้ในกระบวนการอยู่ที่ 0.1 mm/s ถึง 100 mm/s และระยะในการอัดรีดอยู่ในช่วง 2.0 - 3.0 mm

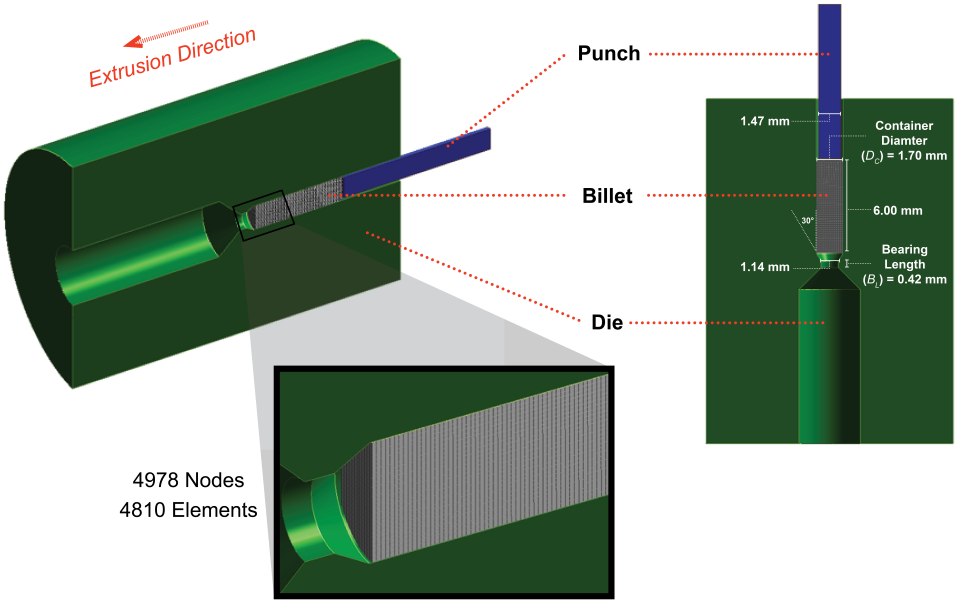

รูปที่ 3 Finite element simulation setup of the micro-extrusion process

2.4 Considered Factors

ตัวแปรหลักที่พิจารณาในโครงการวิจัยนี้ (รายละเอียดอยู่ในภาคผนวก) คือ

2.1 รูปทรงและการวางแนวของแม่พิมพ์ (Tool Geometry and Alignment) ดังแสดงในตารางที่ 1

ตารางที่ 1 ตัวแปรที่พิจารณาเกี่ยวกับ Tool Geometry and Alignment

Factors	**Values**
Extrusion Ratio (ER)	2.43, 9.73, 100.00, 243.25
Die Angle (α)	30°, 45°, 60°, 90°
Billet Length (BL)	3.00 mm, 4.00 mm, 5.00 mm, 5.50 mm, 5.75 mm, 6.00 mm
Bearing Length (LB)	0.50 mm, 1.00 mm, 2.50 mm, 3.00 mm
Die Shift (DS)	0.00 mm, 0.01 mm, 0.05 mm, 0.10 mm

2.2 ขนาดเกรนและการวางตัวของเกรน (Grain Size and Grain Orientation) ดังแสดงในตารางที่ 2

ตารางที่ 2 ตัวแปรที่พิจารณาเกี่ยวกับ Grain Size and Grain Orientation

Factors	**Values**
Grain Sizes	47 μm, 66 μm, 97 μm, 150 μm, 200 μm, 375 μm, 500 μm
Grain Orientations (E11)	-90° to + 90°

2.3 ไทรโบโลยี (Tribology) ดังแสดงในตารางที่ 3

ตารางที่ 3 ตัวแปรที่พิจารณาเกี่ยวกับ Tribology

Factors	**Values**
Friction Models	Coulomb Friction Model, Shear Friction Model, Combined Friction Model
Lubrications	Dry, PAO Lubricant (2.6 mm^2/s Kinematic Viscosity), PAO Lubricant (428.6 mm^2/s Kinematic Viscosity)
Coatings	Uncoated, CrN, TiN, DLC-PVD, DLC-CVD

หมายเหตุ ตัวแปร Strain Rate นั้นไม่มีผลต่อกับการเสียรูปแบบโค้งชิ้นงานอัดรีดขึ้นรูประดับไมโครเนื่องจากเป็นการเสียรูปในอุณหภูมิห้องและช่วงของ Strain Rate ที่ใช้ในกระบวนการนี้

3. Results and Discussions

3.1 Effects of tool geometry and alignment

ผลสรุป รูปทรงและการวางแนวของแม่พิมพ์ ที่ได้จากการจำลองทางไฟไนต์เอลิเมนต์ คือ Die Shift (DS) และ Bearing Length (LB) จะส่งผลโดยตรงต่อการเสียรูปแบบโค้ง และแม่พิมพ์ที่มี Extrusion Ratio (ER) Die Angle (α) Billet Length (BL) และ Bearing Length (LB) สูงจะส่งผลให้ต้องใช้พลังงานในการอัดรีดขึ้นรูปสูง (รายละเอียดอยู่ในภาคผนวก)

3.2 Effects of grain size and grain orientation

ผลสรุปผลกระทบของตัวแปรทางด้านขนาดเกรนและการวางตัวของเกรนที่ได้จากการจำลองทางไฟไนต์เอลิเมนต์ คือ เมื่อขนาดเกรนมีขนาดใหญ่ (1-2 เกรนตามแนวขวางของชิ้นงาน) นั้นขอบเกรนและการวางตัวของเกรนจะเป็นปัจจัยหลักในการทำให้ชิ้นงานเกิดการเสียรูปแบบโค้ง ในส่วนขนาดของเกรนนั้นจะส่งผลโดยตรงต่อพลังงานที่ใช้ในกระบวนการอัดรีดขึ้นรูป ซึ่งเกรนที่มีขนาดเล็กจะมีความแข็งแรงมากกว่าเกรนขนาดใหญ่และจะต้องใช้พลังงานมากขึ้นในการอัดรีดขึ้นรูป (รายละเอียดอยู่ในภาคผนวก)

3.3 Effects of tribology

ผลสรุปผลกระทบของตัวแปรทางด้านไทรโบโลยีที่ได้จากการจำลองทางไฟไนต์เอลิเมนต์ คือ Combined Friction Model นั้นสามารถใช้ในการจำลองพฤติกรรมแรงเสียดทานที่เกิดขึ้นในกระบวนการอัดรีดขึ้นรูปได้ดีกว่า Coulomb Friction Model กับ Shear Friction Model นอกจากนี้แล้ว Lubrications and Coatings นั้นไม่ส่งผลโดยตรงต่อการเสียรูปแบบโค้ง แต่ค่าสัมประสิทธิ์แรงเสียดทานระหว่างพื้นผิววัสดุจะส่งผลโดยตรงกับพลังงานที่ใช้ในการอัดรีดขึ้นรูป (รายละเอียดอยู่ในภาคผนวก)

Conclusions and Future Work

โครงการวิจัยนี้ได้ใช้การจำลองทางไฟไนต์เอลิเมนต์ในการศึกษาถึงอิทธิพลของตัวแปรหลัก คือ รูปทรงและการวางแนวของแม่พิมพ์ ขนาดเกรนและการวางตัวของเกรน และไทรโบโลยี ต่อการเสียรูปแบบโค้งของชิ้นงานที่ถูกอัดรีดขึ้นรูปในระดับไมโคร และพลังงานที่ใช้ในกระบวนการอัดรีดขึ้นรูป โดยผลการจำลองสรุปได้ว่า ตัวแปรหลักที่ส่งผลต่อการเสียรูปแบบโค้ง คือ Die Shift (DS) Bearing Length (LB) และ Grain Size and Grain Orientation เมื่อขนาดของเกรนมีขนาดใหญ่ (จำนวนเกรนประมาณ 1-2 เกรนต่อแนวขวางของชิ้นงาน) และเมื่อเพิ่มค่าของตัวแปรเหล่านี้จะทำให้พลังงานที่ใช้ในกระบวนการอัดรีดขึ้นรูปสูงขึ้น Extrusion Ratio (ER) Die Angle (α) Billet Length (BL) Bearing Length (LB) และ Coefficient of Friction (COF)

โดยผลที่ได้จากงานวิจัยในโครงการนี้จะนำไปใช้ต่อยอดในการออกแบบและควบคุมขนาดของเกรน การเรียงตัวของเกรน เพื่อควบคุมความโค้งของชิ้นงานในระดับไมโครให้ได้ตามที่ต้องการโดยไม่เกิดการสูญเสีย ซึ่งในอนาคตนั้น การเปลี่ยนแปลงรูปร่างของชิ้นงาน การเปลี่ยนแปลงเกรดของวัสดุอะลูมิเนียม (อาทิเช่น อะลูมเนียมเกรด 7075) การเปลี่ยนแปลงชนิดของวัสดุน้ำหนักเบา (Lightweight Materials) การใช้วัสดุต่างชนิดกัน (Dissimilar Materials) จะสามารถทำการศึกษาวิจัยได้โดยอิงจากองค์ความรู้ที่ได้จากโครงการวิจัยนี้ นอกจากนี้แล้ว การออกแบบเกรนในลักษณะที่เป็น Single Crystal ด้วยวิธีการ Grain Selector นั้นจะสามารถนำมาใช้ต่อยอดจากองค์ความรู้ที่ได้รับจากโครงการวิจัยนี้เพื่อนำประยุกต์ใช้ในอุตสาหกรรมต่าง ๆ ได้ อาทิเช่น อุตสาหกรรมอากาศยาน อุตสาหกรรมยานยนต์ อุตสาหกรรมอิเล็กทรอนิกส์ อุตสาหกรรมการแพทย์ เป็นต้น

Appendices

Accepted Journal Publications

Preedawiphat, P.; Mahayotsanun, N.; Sucharitpwatskul, S.; Funazuka, T.; Takatsuji, N.; Bureerat, S.; Dohda, K. Finite Element Analysis of Grain Size Effects on Curvature in Micro-Extrusion. *Appl. Sci.* **2020**, *10*, 4767. https://doi.org/10.3390/app10144767.

Sucharitpwatskul, S.; Mahayotsanun, N.; Bureerat, S.; Dohda, K. Effects of Tool Coatings on Energy Consumption in Micro-Extrusion of Aluminum Alloy 6063. *Coatings* **2020**, *10*, 381. https://doi.org/10.3390/coatings10040381.

Sucharitpwatskul, S.; Mahayotsanun, N.; Mahabunphachai, S.; Funazuka, T.; Takatsuji, N.; Dohda, K., Effects of Friction Models, Geometry and Position of Tool on Curving Tendency of Micro-Extrusion 6063 Aluminum Alloy Pins. *Key Engineering Materials* **2017**, *739*, 135-142.https://doi.org/10.4028/www.scientific.net/KEM.739.135.

Under Reviewed Journal Publications

Sucharitpwatskul, S.; Mahayotsanun, N.; Bureerat, S.; Dohda, K. Energy Consideration in The Micro-Extrusion of Aluminum Alloy 6063. *Journal of Micro and Nano-Manufacturing.*

Sucharitpwatskul, S.; Mahayotsanun, N.; Bureerat, S.; Dohda, K. Effects of Tool Geometry and Alignment in Micro-Extrusion of Aluminum Alloy. *International Journal of Precision Engineering and Manufacturing.*

Conference Publications

Sucharitpwatskul, S.; Mahayotsanun, N.; Mahabunphachai, S.; Takatsuji, N.; Dohda, K. In *Effect of Die Shift on Curvature of Micro-Extruded Pins*, The 2017 World Congress on Micro and Nano Manufacturing, Taiwan, Taiwan, 2017; pp 63-66.

Journal:	Applied Sciences
Journal Impact Factor:	2.474
Paper Title:	Finite Element Analysis of Grain Size Effects on Curvature in Micro-Extrusion
DOI:	10.3390/app10144767

applied sciences

MDPI

Article

Finite Element Analysis of Grain Size Effects on Curvature in Micro-Extrusion

Pavaret Preedawiphat [1], Numpon Mahayotsanun [1,*], Sedthawatt Sucharitpwatskul [2], Tatsuya Funazuka [3], Norio Takatsuji [4], Sujin Bureerat [1] and Kuniaki Dohda [5]

1 Department of Mechanical Engineering, Faculty of Engineering, Khon Kaen University, 123 Moo 16 Mittraphap Rd., Nai-Muang, Muang, Khon Kaen 40002, Thailand; pavaret.pp@gmail.com (P.P.); sujbur@kku.ac.th (S.B.)
2 National Metal and Materials Technology Center (MTEC), National Science and Technology Development Agency (NSTDA), Pathum Thani 12120, Thailand; sedthaws@mtec.or.th
3 Academic Assembly Faculty of Engineering, University of Toyama, 3190 Gofuku, Toyama-shi, Toyama 930-8555, Japan; funazuka@eng.u-toyama.ac.jp
4 Academic Assembly Faculty of Sustainable Design, University of Toyama, 3190 Gofuku, Toyama-shi, Toyama 930-8555, Japan; takatuji@sus.u-toyama.ac.jp
5 Department of Mechanical Engineering, Northwestern University, 2145 Sheridan Road, Evanston, IL 60208, USA; dohda.kuni@northwestern.edu
* Correspondence: numpon@kku.ac.th

Received: 4 June 2020; Accepted: 8 July 2020; Published: 10 July 2020

Abstract: The precision and accuracy of the final geometry in micro-parts is crucial, particularly for high-value-added metallic products. Micro-extrusion is one of the most promising processes for delivering high-precision micro-parts. The curving tendency observed in micro-extrusion parts is a major concern, significantly affecting the final part geometry. The purpose of this paper was to investigate the driving mechanism behind the curvature in micro-extrusion at room temperature. A finite element (FE) simulation was carried out to observe the influential primary factors: (1) grain size, (2) grain boundary, (3) grain orientation, and (4) bearing length of a 6063 aluminum alloy. The Extrusion Curvature Index (*ECI*) was also established to indicate the level of curvature in micro-extruded parts. The results showed that the grain boundary at the high strain and die opening area was the dominant factor for single-grain conditions. The interactive effects of the grain boundary and grain orientation also affected the curvature under single-grain conditions. If the number of grains across the specimen increased up to 2.7 (poly-grains), the curvature effect was dramatically reduced (the pins were straightened). For all conditions, the curvature in micro-extrusion could be eliminated by extending the bearing length up to the exit diameter length.

Keywords: aluminum alloy; curvature; grain size; micro-extrusion; finite element analysis

1. Introduction

The global demand for end-uses of aluminum products has been rising [1]. One of the potential areas where one can add value for aluminum is in micro-products development [2]. An example of a micro aluminum product is a micro-gear [3]. Not only are aluminum micro-parts suitable for lightweight miniaturized applications in the automotive and electronic industries, but they can also be produced for biomedical applications (rod, wire, ribbon, screw, and tube drawing shapes) [4]. Many of the processing techniques can be applied to produce aluminum micro-parts [5]. Machine developments and manufacturing systems were also developed in this area [6]. Recent trends in micro-forming processes that are particularly suitable for lightweight materials (aluminum, titanium, and magnesium alloys) have been reviewed [7]. Most of the macro-forming processes could be downsized to micro-forming

processes, with some challenges due to the reduced scale [8]. The concept of traditional extrusion to produce sub-millimeter parts by using the micro-extrusion process was developed [9]. An example of aluminum micro-extruded components was also investigated [10].

In macro-extrusion, one of the relevant issues related to the grain size is surface grain coarsening [11]. The effects of the grain size can also be commonly observed and becomes quite problematic in micro-extrusion. The main challenge in micro-forming processes is the size effects that show a reduced geometrical accuracy, flow stress, and an increase in the scattering of the flow stress and part geometry when the grain size is comparable to the specimen size [12]. An inverse relationship between the yield stress of aluminum and its grain size has been observed [13]. This relationship follows the Hall–Petch effect [14]. A scaling model taking into account the specimen/feature size in micro-forming was proposed [15]. The influence of single-grain orientations affected deformation [16]. The micro-extruded pins were curved when the grain size was enlarged so as to be close to the specimen size [17].

Tribology plays an essential role in size effects in micro-forming processes [18]. The tribological characteristics in this scale could be described by using the open and closed lubricant pockets model. The friction condition depended on the specimen size in the micro-extrusion process [19]. The tool-billet interface of the micro-extrusion process under both static and dynamic conditions was observed [20]. The tribological phenomena in various micro-forming processes were significantly influenced by the size effects [21]. The interfacial friction and grain size effects were dependent [22]. The conventional material model could not be applied in micro-extrusion. The experimental and numerical studies showed that the interactions of the friction interfaces, material properties, and size effects contributed to the forming loads and parts geometry [23]. An approach to determine the stress–strain curve in micro-extrusion by taking into account the friction factor was proposed [24]. A forming load prediction taking into account the surface area was also developed [25]. The microstructural evolution in the open-die forging/extrusion process was investigated, and the results showed that the grain size and specimen size influenced the microstructures [26]. An upper bound approach to predict the forming behavior in the open-die forging/extrusion process was also proposed [27]. The role of subgrains larger than the specimen diameter contributed to a reduced flow stress in the micro-compression tests [28]. In the micro-extrusion of both copper and aluminum alloys, the flow stress decreased along with the surface grain [29]. If the cavity width in micro-coining consisted of only one grain, the grain would be fragmented into smaller sizes along the extrusion direction [30].

The area of interest in this research was the effects of the grain size on the curving behavior of micro-extruded pins. Generally, extrusion profiles are curved due to the unbalanced flows/velocities in macro-extrusion [31]. The modeling of the curved aluminum profiles has also been proposed [32]. A finite element analysis of the die design and optimization for a balanced flow in extrusion has also been used [33]. However, this was not the case in micro-extrusion. Here, the curving behavior was found when the grain size approached the billet size. Crystal plasticity finite element (CPFE) simulations were conducted to demonstrate that the grain orientations played an important role [34]. Although both grain sizes and grain orientations were found to affect the deformation behaviors, it was still unclear what the mechanism was that drove the micro-extrusion part to curve and how the curving direction was dictated. This study explored the interactive influences of the grain size, grain boundary, grain orientation, and bearing length on the micro-extrusion of aluminum alloy. A finite element simulation was utilized to carry out the interactive effects of these factors. Understanding the curving mechanism in the micro-extrusion was essential to the final geometry control and necessary for producing high-precision micro-parts.

2. Materials and Methods

2.1. Micro-Extrusion Experiment and Simulation

The principle of the micro-extrusion process was similar to that of the traditional extrusion process but was carried out at room temperature, while also reducing the millimeter-sized billets to a few millimeter-sized or micro-sized parts. A horizontal type high-speed micro-extrusion machine (Figure 1) was used in this study to push the prepared 6.00-mm billets having a 1.70-mm diameter down to an extruded pin having a 1.14-mm diameter at room temperature. The punch and die material was SKD11. Aluminum alloy 6063 was selected as a billet material because it is a commonly used material in aluminum extrusion. The billet specimen was prepared by hot extrusion and machining, and the grain size of the non-annealed billets was 66 μm, with a hardness value of 30.7 HV. The material flow curve of the billet specimen obtained by the compression test is shown in Figure 2 (σ is stress, υ is Poisson's ratio, E is Young's moduli, G is shear moduli, and ε is strain).

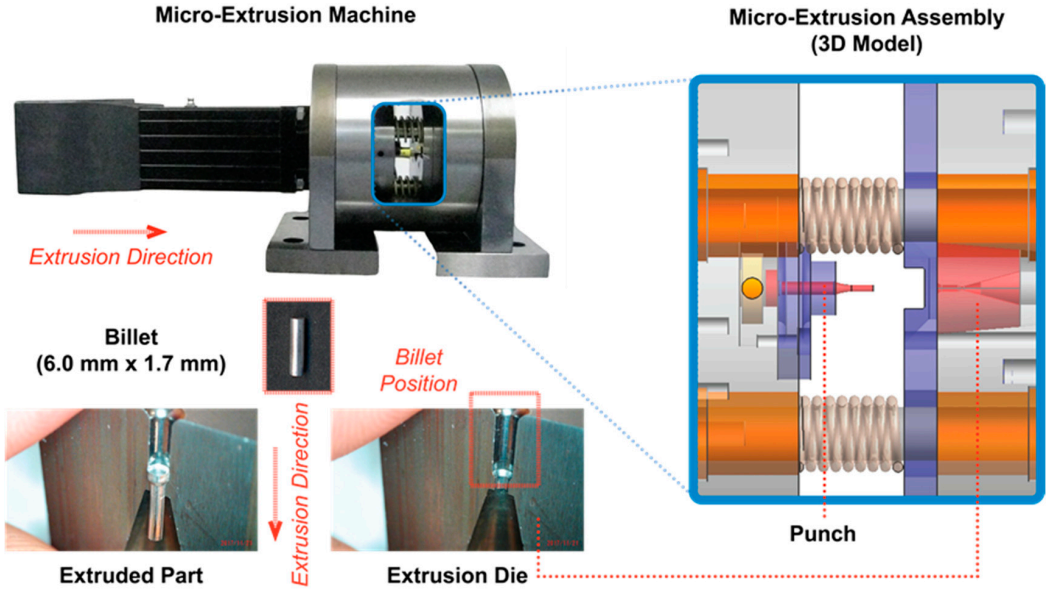

Figure 1. The micro-extrusion machine with the assembly model, and the micro-extrusion setup.

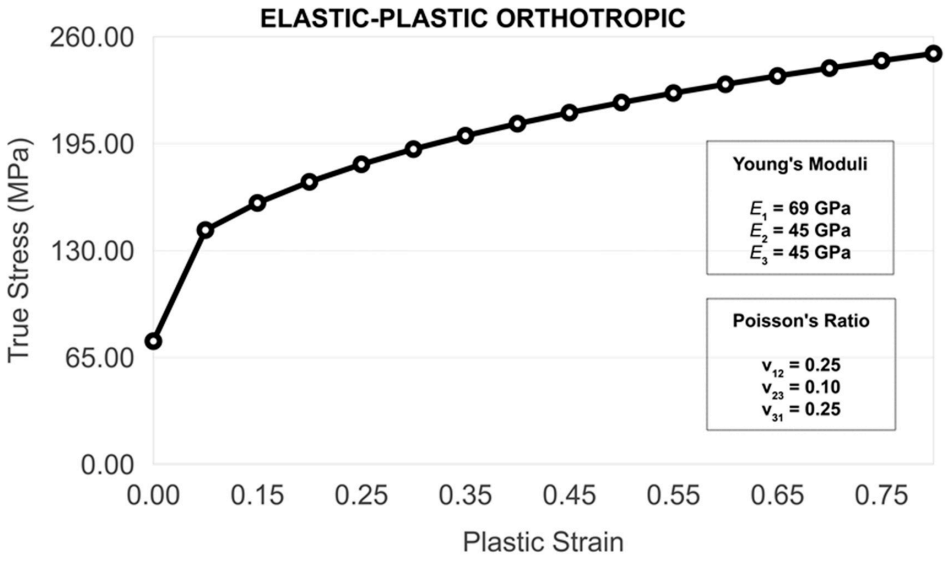

Figure 2. The stress strain curve of the aluminum alloy 6063 having a 66-μm grain size.

A finite element (FE) model was developed to determine how the size effects (grain boundary and grain orientation) affected the curving behavior of the micro-extruded parts by using MSC.Marc 2019 (Lagrangian). The model was a 2D axisymmetric, four-node fully integrated element, with no heat transfer, as seen in Figure 3. A total number of 4978 nodes and 4810 elements were generated. The tools (punch and die) were set to be rigid bodies. The billet was set to be a deformable body having the power-law material model, as shown in Equation (1):

$$\sigma = k \cdot \varepsilon^n, \tag{1}$$

where σ is the flow stress, k is the material constant, ε is the true strain, and n is the strain-hardening exponent. Since the maximum strain rate used in this work was 100 s^{-1} at room temperature, the effects of the strain rate on the flow stress were considered minimal, as presented in the work of Ye et al. [35]. Thus, the strain-rate sensitivity was not included in Equation (1). The flow stress-true strain curves were calculated from the cold compression tests. The material constants for aluminum alloy 6063 having a 66-µm grain size were: k = 168.40 MPa and n = 0.30. The lubricant (2.606 mm^2/s kinematic viscosity) was applied at the billet-tool interfaces. The FE simulation was estimated by comparing it with the three micro-extrusion experiments, as described in Table 1.

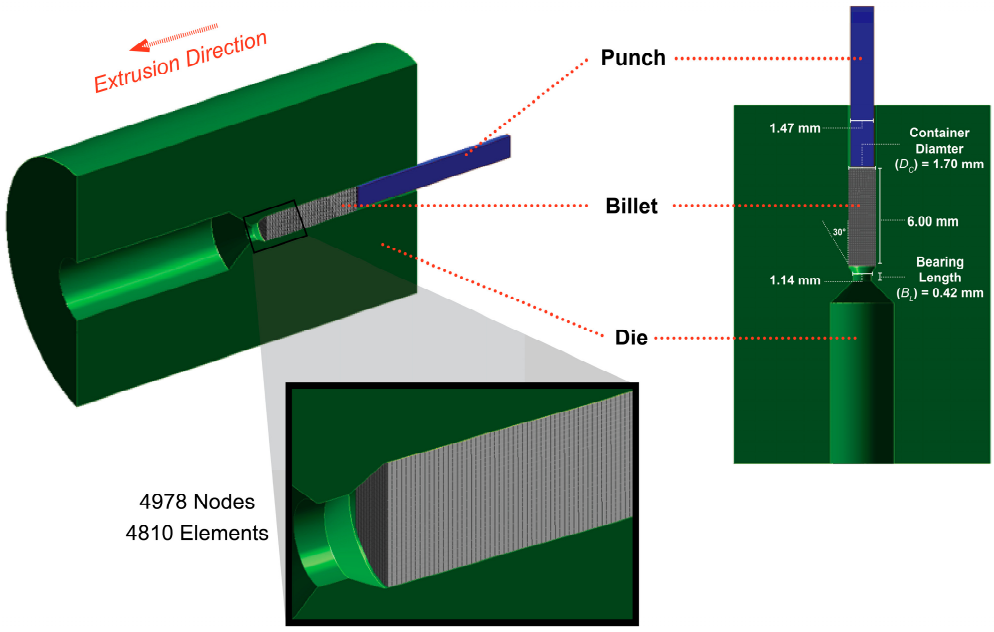

Figure 3. The finite element simulation setup of the micro-extrusion process.

Table 1. Experimental validation conditions for the finite element (FE) model.

Condition	Lubrication	Tool Coating	Coefficient of Friction	Extrusion Speed
Test A	PAO Lubricant (2.6 mm^2/s Kinematic Viscosity)	Uncoated	0.45	0.10 mm/s
Test B	PAO Lubricant (428.6 mm^2/s Kinematic Viscosity)	Uncoated	0.25	0.10 mm/s
Test C	Dry (No Lubricant)	DLC (PVD)	0.11	100 mm/s

In the validation conditions, the 66-µm grain size billet was extruded from a diameter of 1.70 mm to 1.14 mm with the 2.00-mm punch stroke. The ASTM E112 standard was used to measure the average grain size of the billet material. The main differences among these conditions were the

friction conditions of the tool-billet interfaces and the extrusion speeds. The combined friction models (Coulomb and shear friction models) were used at the tool-billet interfaces, as shown in Equation (2):

$$f = \mu_s N \ (if \ \mu_s N < \tau), f = \tau \ (if \ \mu_s N \geq \tau), \tag{2}$$

where f is friction force, μ_s is the static friction coefficient, N is the normal load, and τ is the shear friction force. Note that the values of the coefficient of frictions were obtained by trials and errors in the FE simulations. The results comparison between the FE simulations and experiments is illustrated in Figure 4. The considered tests (A, B, and C) had different friction pairs (different COF values). The FE results matched well with those of the experiments, implying that the material model Equation (1) and friction model Equation (2) were suitable for the micro-extrusion process.

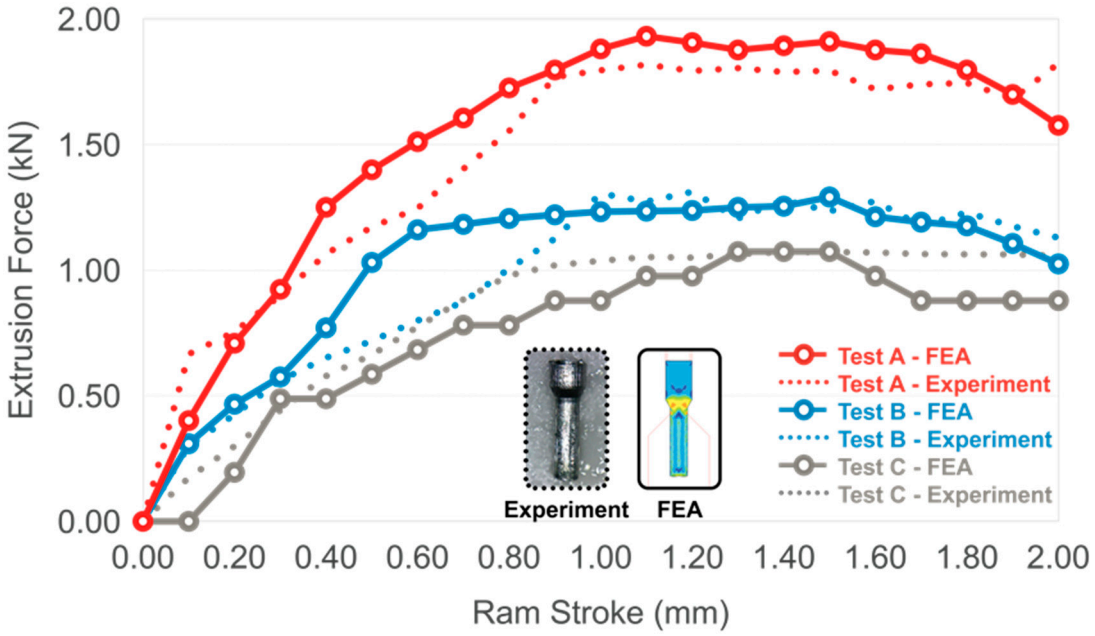

Figure 4. The results comparison between the experimental and FE micro-extrusion tests by using the 66-μm grain-size billets under different friction conditions.

2.2. Considered Grain Sizes, Grain Boundaries, and Grain Orientations

The initial billet textures resulted from the specimen preparation processes (hot extrusion at 460 °C, followed by annealing) for achieving the desired grain sizes (47 μm, 66 μm, and 97 μm), and their grain size distributions are illustrated in Figure 5. Three additional grain sizes were investigated, in order to look at the influences of poly-grain to single-grain conditions, as seen in Figure 6. The grain shapes used here were selected on purpose and were based on the study of Roters et al. [36]. Grain shapes with a face-centered cubic (FCC) crystal structure, clearly showing individual grains, were selected for this study. The grain sizes and shapes (boundaries) were modeled in the FE simulation based on the assumption that there were no annealing twins. The Average Grain Size (G_A) was the average maximum width of each grain across the billet specimen. The Grain Size Ratio (G_R) was the Average Grain Size (G_A) over the billet diameter (1.70 mm). Since the material data of these set grains were not available, the prediction of the material flow curves was carried out based on the existing stress-strain curves (47 μm, 66 μm, and 97 μm) from the compression tests. The estimated material flow curves of these enlarged grains are shown in Figure 7, and their power-law model constants are described in Table 2.

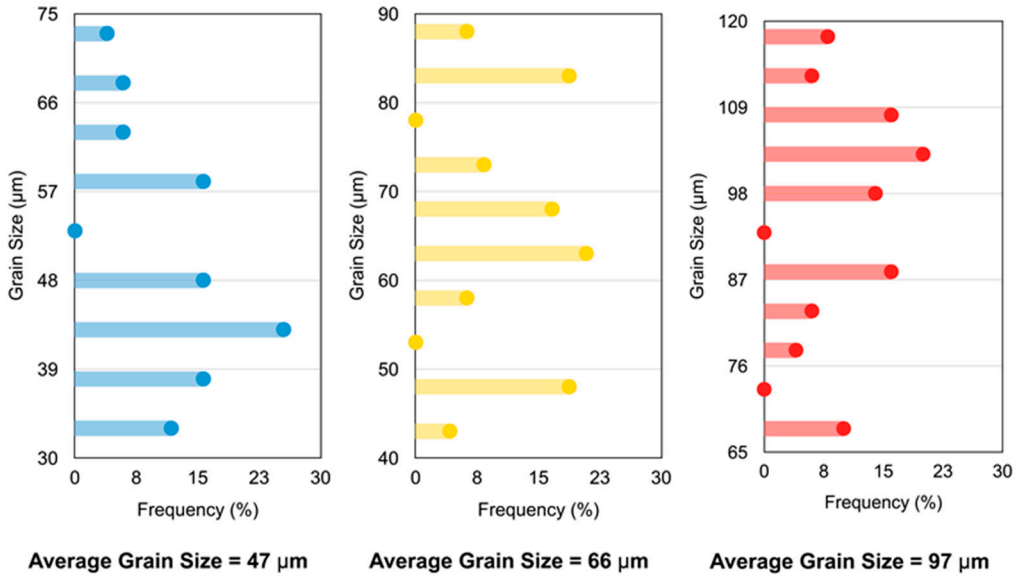

Figure 5. The grain size distributions of the 47-μm, 66-μm, and 97-μm grains.

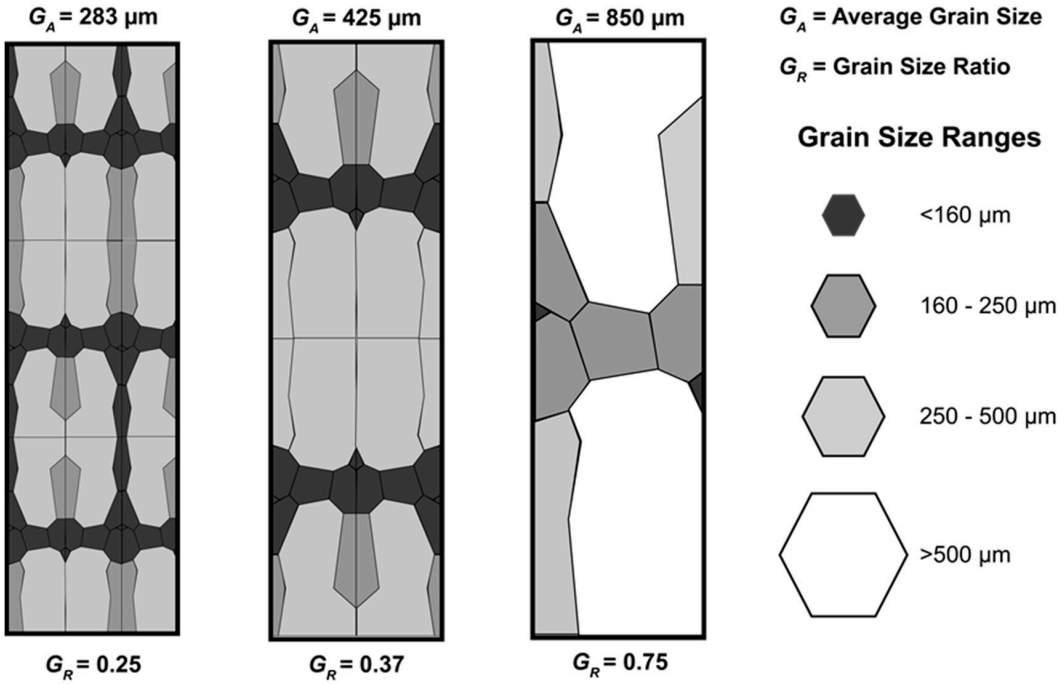

Figure 6. The considered grain sizes and shapes (boundaries) in this study.

Table 2. The material constants in the power-law model of the enlarged grains [37].

Average Grain Size	Material Constant (*k*)	Strain Hardening Exponent (*n*)	Source of Data [37]
47 μm	265.30 MPa	0.27	Compression Test
66 μm	168.40 MPa	0.30	Compression Test *
97 μm	163.10 MPa	0.25	Compression Test
150 μm	113.00 MPa	0.23	Prediction
200 μm	94.12 MPa	0.23	Prediction
375 μm	63.13 MPa	0.21	Prediction
500 μm	52.58 MPa	0.20	Prediction

* The *k* and *n* values here were used in Equation (1) to obtain the material flow curve of the 66-μm grain size.

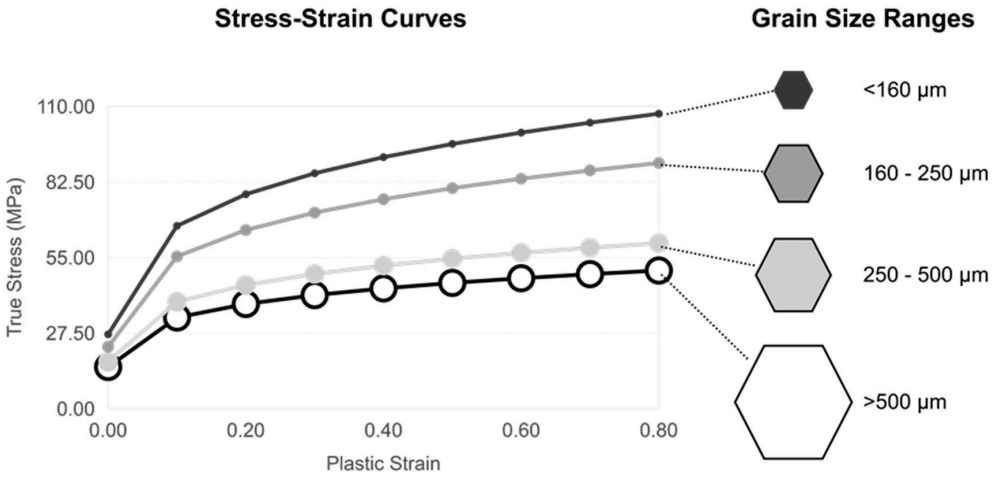

Figure 7. The estimated stress-strain curves of the considered grain sizes.

The grain sizes in the simulation did not reflect typical microstructures. However, the large grain sizes and grain boundaries in this study were specifically chosen to determine their influences on the curvature and if they could be potentially produced by using the grain selector method in our parallel study (single-crystal parts manufacturing). A few examples of the grain selection method can be found in the cited papers [38–41]. Since the stress-strain curves strongly depend on the loading axis, single crystals with different orientations would yield different stress-strain curves. In this study, instead of changing the loading axis to obtain different grain orientations, the stress-strain curves were oriented in set degrees away from the loading axis. In Figure 8, the loading axis (extrusion direction) was the x-axis. Since the material model was elastic-plastic orthotropic, the orientation of the stress-strain curves could be varied by changing the orthotropic elastic principal direction (E11). If E11 of any particular grain rotated (or changed orientation), its stress-strain curve changed. The grain orientation was described by the plane angle subtended by an arc along the x-axis (radians). For instance, if E11 equals 0 radians, the grain orientation is aligned with the x-axis (extrusion direction). If E11 equals 0.79 radians, the grain orientation is rotated 45° counterclockwise from the x-axis.

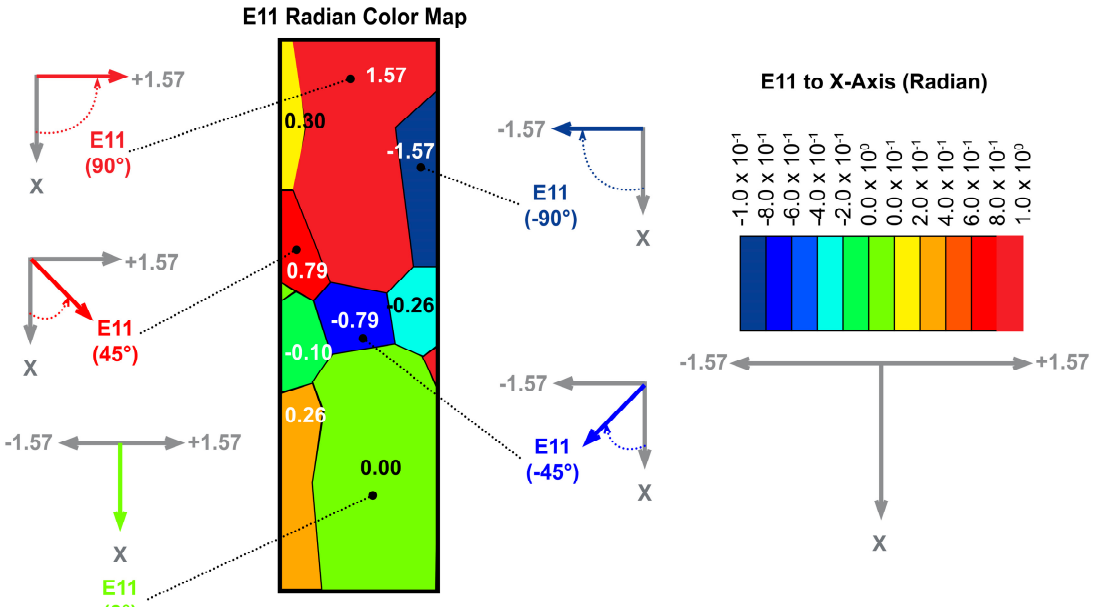

Figure 8. The random grain orientations via rotating the orthotropic elastic principal direction (E11) along the x-axis.

2.2.1. Grain Orientations

Two cases that had rectangular grain sizes and shapes were established in order to only investigate the grain orientation effects, as illustrated in Figure 9. In the first case (EX1), all of the grains were oriented along the x-axis (0.00 radians). For the second case (EX2), the grain sizes and boundaries were the same as those of EX1, but the only difference was the orientation of the bottom grain (E11 rotated 75° counterclockwise from the x-axis).

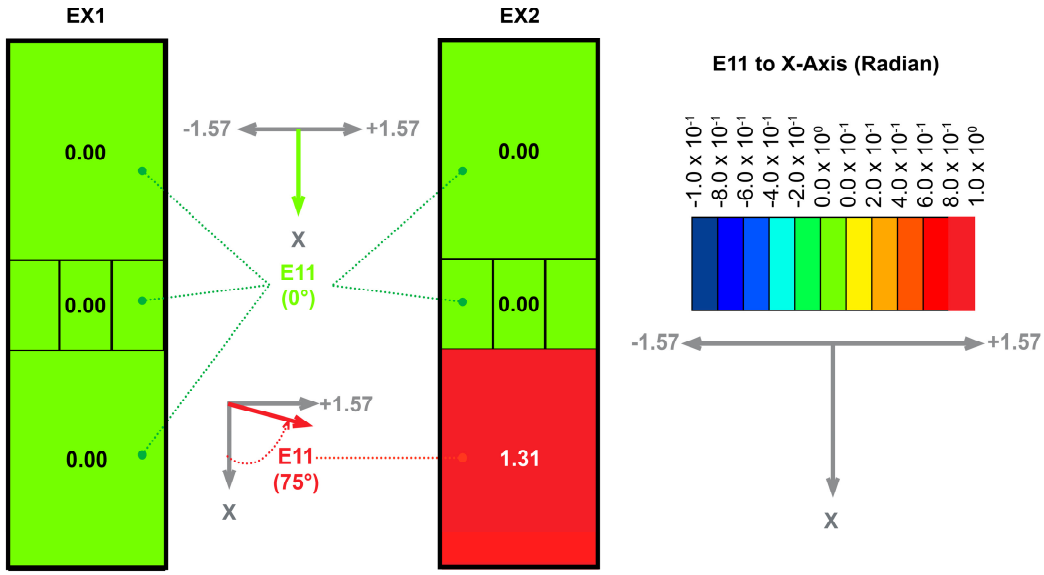

Figure 9. The two cases having the same grain sizes and shapes except for their grain orientations.

2.2.2. Grain Boundaries and Grain Orientations

In reality, those rectangular grain boundaries did not exist, so the referenced literature grain boundaries (Figure 8) were investigated throughout this study. However, the systematic way of evaluating the interactive effects of grain boundaries and grain orientations was developed as follows.

In Figure 10, all four cases (LG1 to LG4) had the same grain sizes and grain boundaries, but the only difference was the grain orientations of the bottom grains. The grain orientation was rotated 0° (LG1), 45° (LG2), 90° (LG3), and −45° (LG4) along the x-axis. In Figure 11, the influences of the top and bottom grain orientations were studied (LG5), where the grains were oriented −14.3° along the x-axis. The influences of the top, middle, and bottom grain orientations were observed in LG6. The grain orientation effects of only the middle grain (LG7) were examined. In LG8, only the middle three grains were rotated by −14.3° along the x-axis. In Figure 12, the bottom grains were turned by −14.3° along the x-axis for all four cases. The main difference was the grain orientations of the middle grain (LG10), the middle three grains (LG11), and the top and middle three grains (LG12).

2.2.3. Grain Sizes and Grain Boundaries

The variations of the average grain sizes (G_A) were established in Figure 13 to observe the coupling effects of the grain sizes and grain boundaries. Note that all four cases had the same grain orientation (0° with respect to the x-axis). Figure 14 displays the mesh elements of the enlarged grains in the finite element simulation.

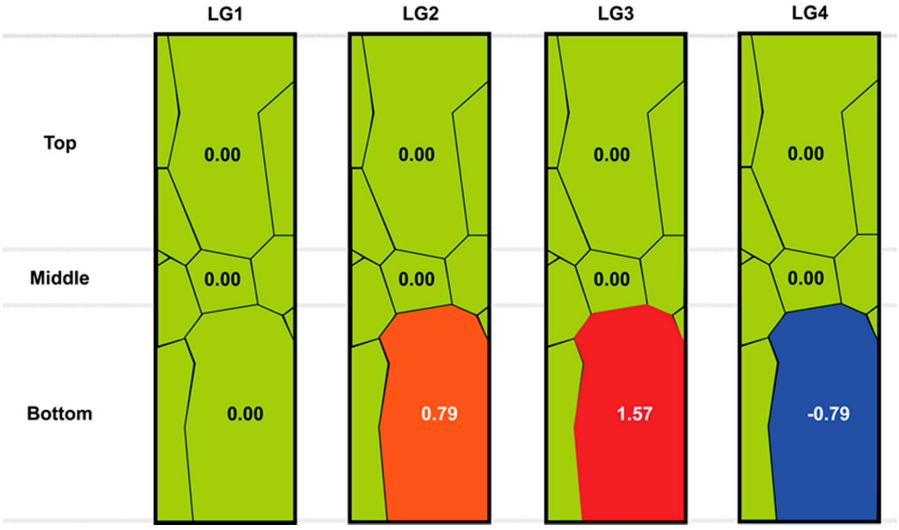

Figure 10. The grain orientations of the four considered cases (LG1 to LG4).

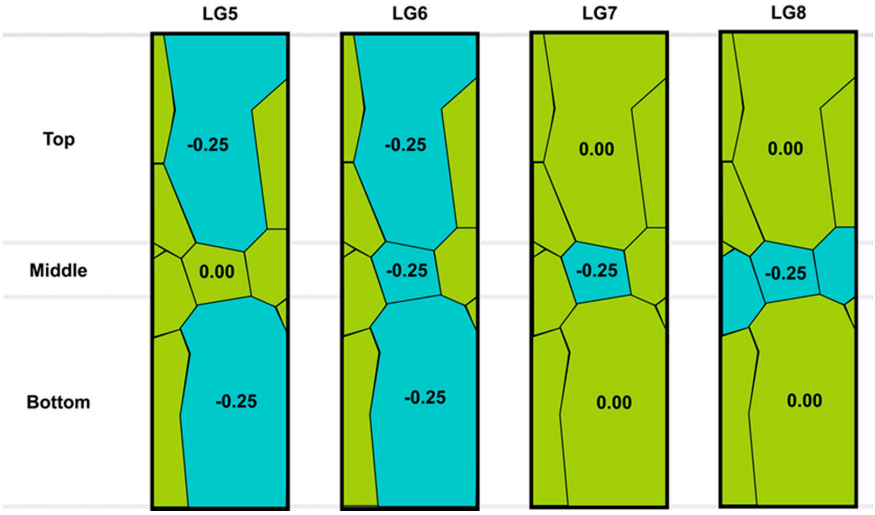

Figure 11. The grain orientations of the four considered cases (LG5 to LG8).

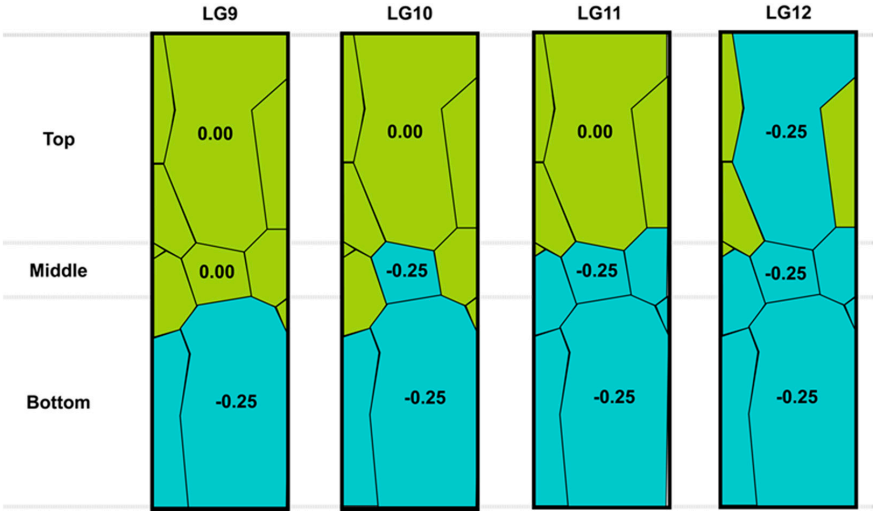

Figure 12. The grain orientations of the four considered cases (LG9 to LG12).

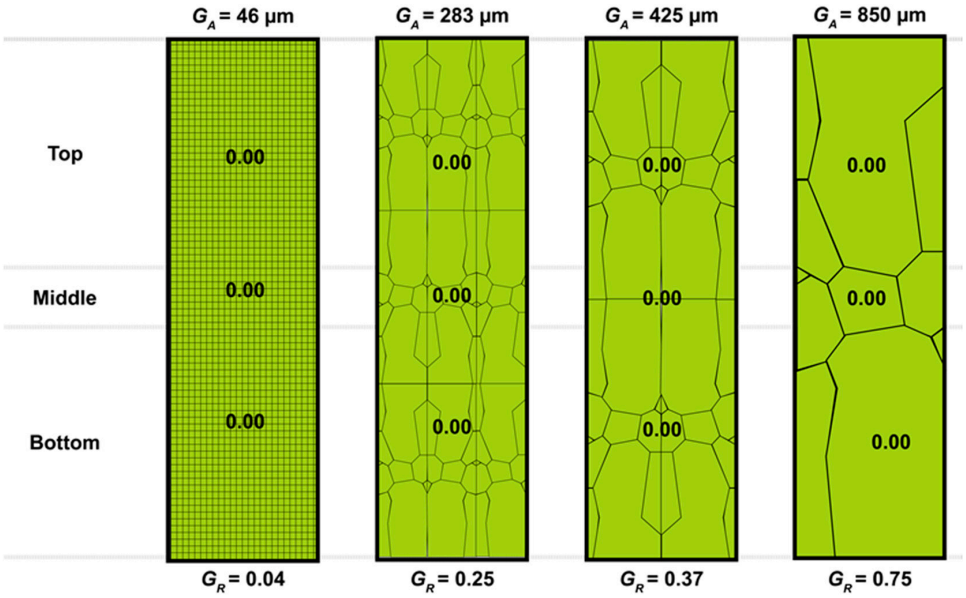

Figure 13. The grain boundaries of the four considered cases (small to large grain sizes) having the same grain orientation.

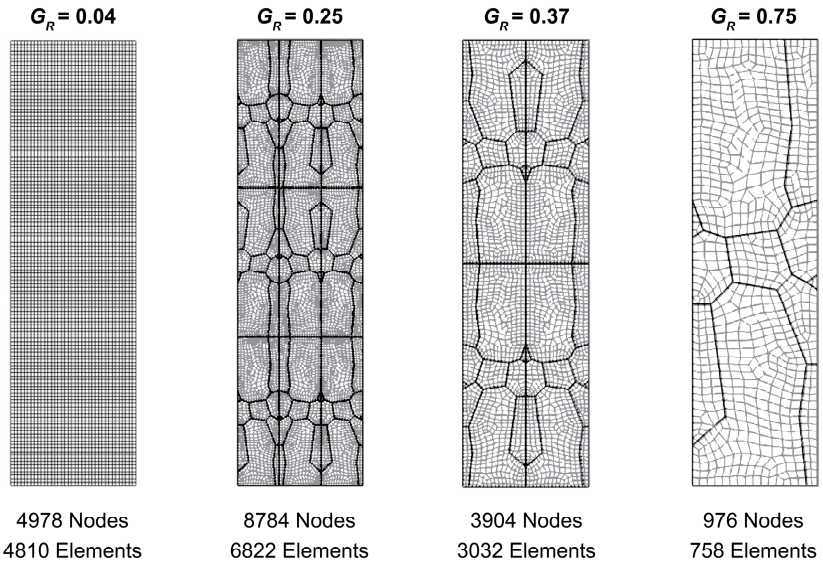

Figure 14. The meshing elements and nodes of the studied grain sizes.

2.2.4. Bearing Lengths

The effects of the bearing length (B_L) were also explored in order to determine how the tool geometry affects the curvature of the micro-extruded pins. Three bearing lengths varied as follows: 0.42 mm (1X), 0.84 mm (2X), and 1.26 mm (3X).

2.2.5. Extrusion Curvature Index

The Extrusion Curvature Index (ECI) was established in order to determine the amount of curvature of the micro-extruded pins, as illustrated in Figure 15. After each extrusion, the curvature point that could fit its inner radius and outer radius to the curvature of the micro-extruded pin was located. The radii were then normalized by the exit diameter (DE), and its inverse value in percentage was the Extrusion Curvature Index (ECI). High values of ECI implied a high degree of curvature. Low ECI values indicated that the micro-extruded pin was rather straight.

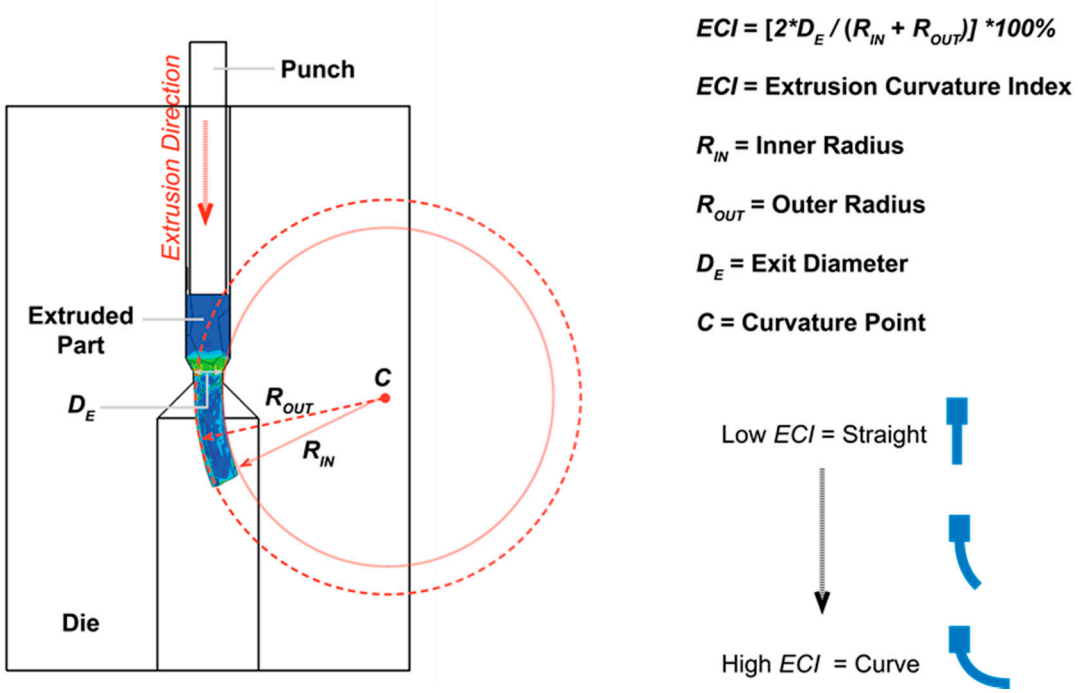

Figure 15. The schematic and calculation of the Extrusion Curvature Index (*ECI*).

3. Results and Discussion

3.1. Effects of Grain Orientations

Figure 16 shows a comparison of the micro-extrusion results between the two cases (EX1 and EX2) having the same grain sizes and grain boundaries, but having different grain orientations of the bottom grains. If all grains were oriented in the same direction (EX1), and the grain sizes and grain boundaries were symmetric along the extrusion direction, there should be no curvature at all. The results of EX1 demonstrated that the FE simulation was valid. The results of EX2 clearly showed that the bottom grain orientation that was rotated 75° with respect to the x-axis caused the micro-extrusion pin to bend (ECI = 4.45%). With no effects of grain sizes and grain boundaries under single-grain conditions, the change in grain orientation could cause the micro-extrusion pin to curve. Regarding the stress distributions, high stresses occurred at high deformation zones (reduction of billet diameter to the outlet diameter). These areas caused the grains to fragment, leading to smaller grain sizes and higher stress values. The simulation results provided effective stress (σ_v) values based on the following equation:

$$\sigma_v = \sqrt{\frac{1}{2}[(\sigma_1 - \sigma_2)^2 + (\sigma_2 - \sigma_3)^2 + (\sigma_1 - \sigma_3)^2]} \quad (3)$$

where σ_1, σ_2, and σ_3 are the principal stresses.

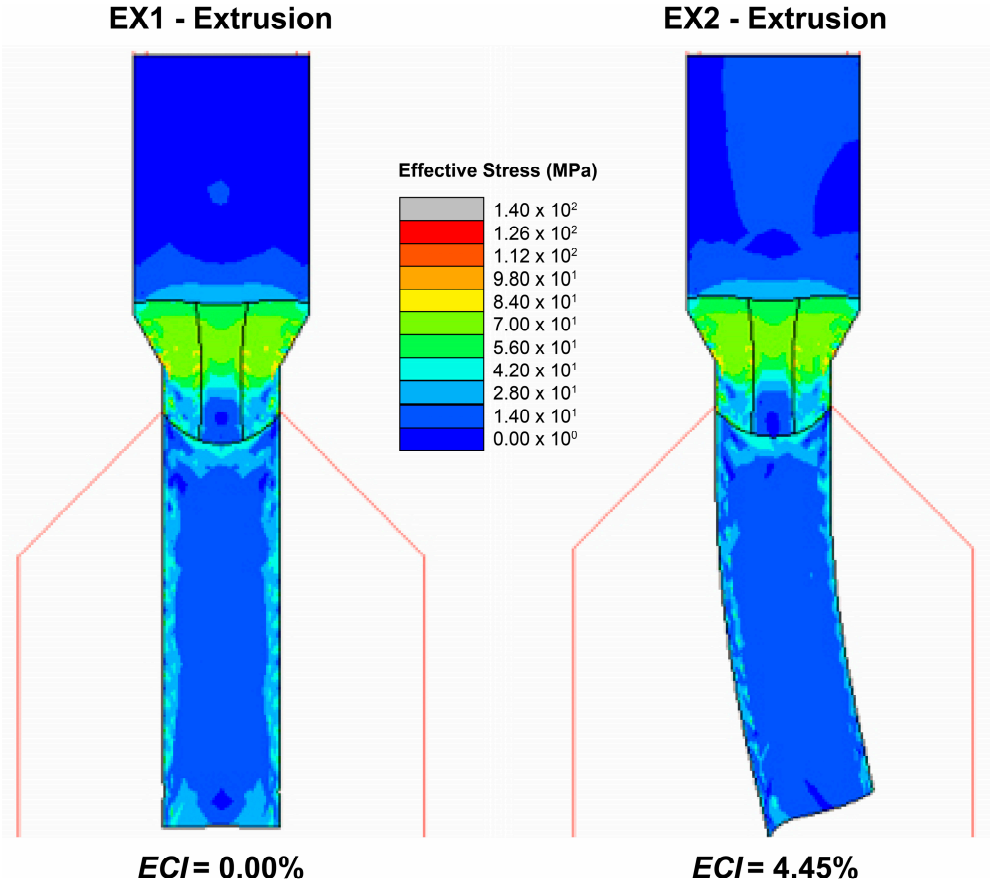

Figure 16. The micro-extrusion results comparison between the EX1 and EX2 conditions.

3.2. *Effects of Grain Boundaries and Grain Orientations*

Figures 17–19 show the FE results of the considered conditions in order to observe the influences of the grain boundaries and grain orientations when the Grain Size Ratio (G_R) was 0.75.

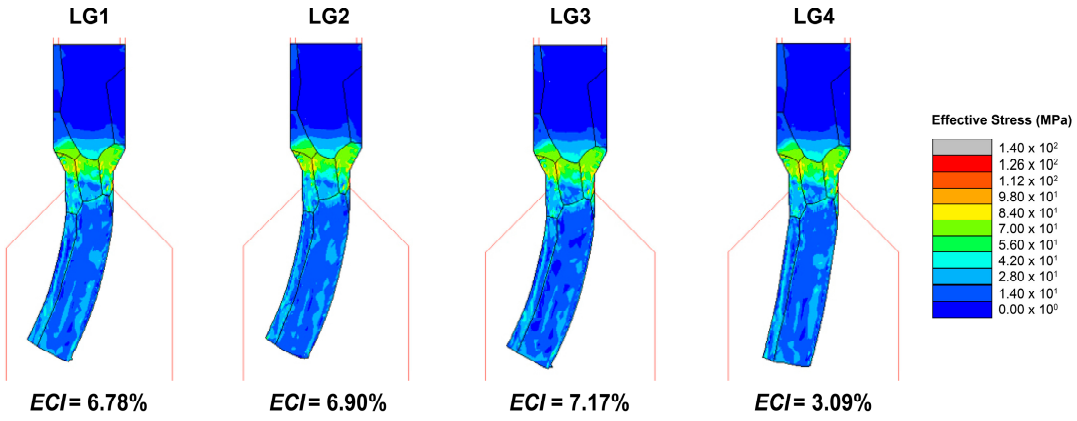

Figure 17. The micro-extrusion results of the considered conditions (LG1–LG4).

In other words, the average number of grains across the specimen was 1.3 (single-grain) under all the conditions. In LG1, all of the grain orientations were along the x-axis, which showed that the micro-extrusion pin was curved. This result indicated that, when there was no influence from the grain orientation, the grain boundaries alone could significantly affect the curvature. It could be observed that the grain boundaries were not symmetric along the x-axis, causing the specimen to flow

nonuniformly into the extrusion die. This behavior implied that the asymmetric grain boundaries were the primary driving mechanism of the bending. In LG2, the effect of the grain orientation (+45° from the x-axis) of the bottom grain was coupled with the influence of the asymmetric boundaries. The ECI values of both LG1 and LG2 were similar (same curvature); thus, the effect of grain orientation was not observed here. However, when the bottom grain orientation was rotated +90° from the x-axis (LG3), the ECI values slightly increased from 6.90% to 7.17%. As a result, the grain orientation must be dramatically changed in order to see the curvature effect. When the bottom grain orientation was rotated−45° from the x-axis (or −90° opposite to LG2), the ECI values were reduced from 6.90% to 3.09%, which helped to straighten the micro-extrusion pin. This result also confirmed that the grain orientation must be significantly changed in order to see the curvature effect. In the direction of the curvature, the curvature increased with an increase in the amount of grain orientation mismatch. However, if the orientation mismatch was in the opposite direction to the curvature, the curvature decreased according to the amount of grain orientation mismatch.

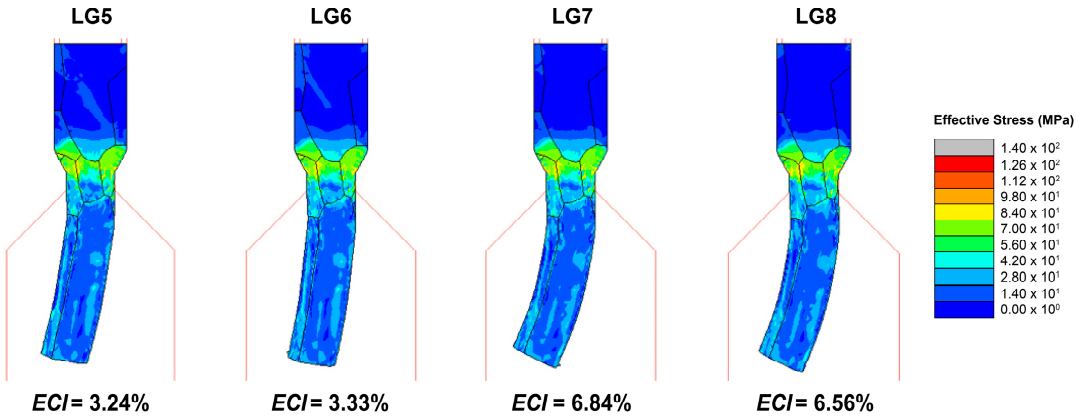

Figure 18. The micro-extrusion results of the considered conditions (LG5–LG8).

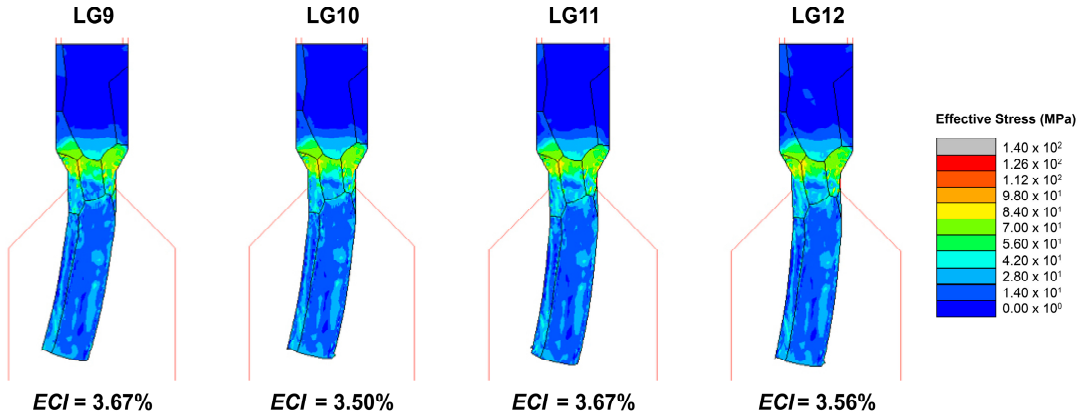

Figure 19. The micro-extrusion results of the considered conditions (LG9–LG12).

Figure 18 shows the conditions (LG5 to LG8) that take into account the effects of the grain orientations from the middle and top grains. Considering LG5 and LG6, it could be noted that both the middle and top grain orientations did not affect the curvature. Similarly, the middle grain orientations (LG7 and LG8) did not affect the curvature when compared with LG1. As a result, the bottom grain orientations significantly affect the curvature. Since the bottom grain was located at the high deformation (reduced diameter) and opening area, this implied that only the grain orientations at the high strain and opening area influenced the curvature. This phenomenon could also be observed in Figure 19, where the middle and top grain orientations did not show any effects on the curvature.

Based on the results from Figures 16–19, it could be stated that the grain boundary of the high strain and die opening area was the dominating factor for single-grain billet conditions. Since the actual metallic grain shapes were not symmetric and the grain orientations were random, the grain boundary dominated. The combination of the grain shapes (grain boundaries), grain sizes, and grain orientations dictate the direction of the curvature. In the EX2 case, there was only one single grain at the bottom of the billet. As a result, the change of grain orientation (+75° to the extrusion direction) of the bottom grain caused the extruded pin to curve to the right. In the other single-grain cases, the curvature was mainly influenced by the initial bottom grain boundaries. As seen in the LG1 case, the extruded pin was already curved to the left, even when all the bottom grain orientations were 0° to the extrusion direction. When the grain orientations of the large bottom grains were changed in the single-grain cases, the curvature directions were still towards the left, but the amount of curvature (ECI values) changed according to the set grain orientations. The results clearly showed that the initial grain boundaries of the bottom grains significantly affected the curvature directions.

3.3. Effects of Grain Sizes and Grain Boundaries

Figure 20 shows the influences of the grain sizes and grain boundaries on the micro-extrusion, when the grain orientations did not influence any of the conditions. If the Grain Size Ratio (G_R) was reduced from 0.75 to 0.37 or below, the ECI values decreased dramatically. In other words, if the specimen grains moved from 1.3 to 2.7 grains or more, the micro-extrusion pin was straightened. The impact of the grain boundaries could be clearly noticed under the single-grain condition (G_R = 0.75). The influence of the grain boundaries was dramatically reduced when the number of grains increased (G_R = 0.37 and below). Even though the grain orientations were not considered here, it could be stated that the effects were negligible when the number of grains was increased from 1.3 to 2.7 or more, according to the previous results. The grain boundaries that were symmetrical along the extrusion axis were G_R = 0.04 and G_R = 0.37. Both G_R = 0.25 and G_R = 0.75 had asymmetric grain boundaries along the centerline. According to Figure 20, it could be observed that the increased number of grain sizes straightened the extruded pins. The results implied that the asymmetry of grain boundaries did not have an effect on the curvature in the multi-grain cases.

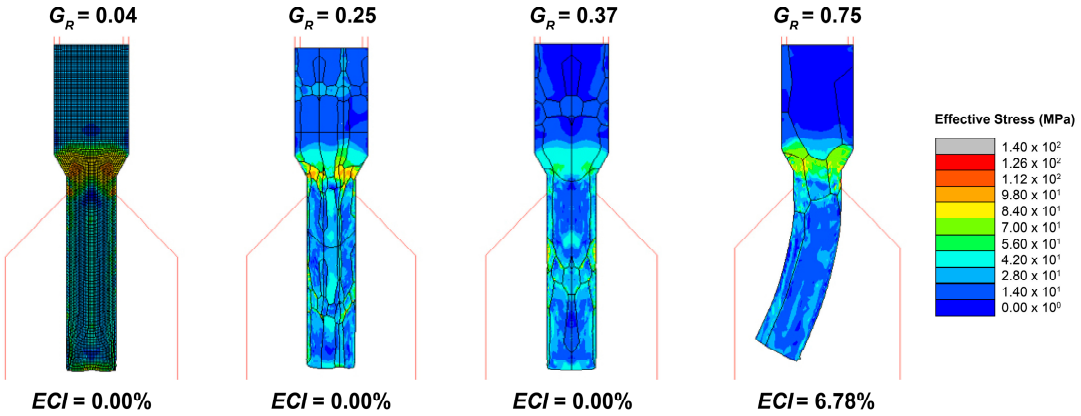

Figure 20. The results comparison among different grain sizes.

3.4. Effects of Bearing Lengths

Figure 21 shows the effects of the bearing lengths (B_L) on the curvature of single-grain conditions (G_R = 0.75). The ECI values decreased when the bearing lengths increased. In other words, if the bearing length was extended further, it could help strengthen the micro-extruded pins. If the B_L value was increased up to 1.26 mm, which was slightly larger than the exit diameter (1.14 mm), it could almost eliminate the curvature in the micro-extrusion. As a result, the extension of the bearing lengths

(B_L) from the high strain and opening area could help reduce the curvature effects influenced by the grain sizes, grain boundaries, and grain orientations.

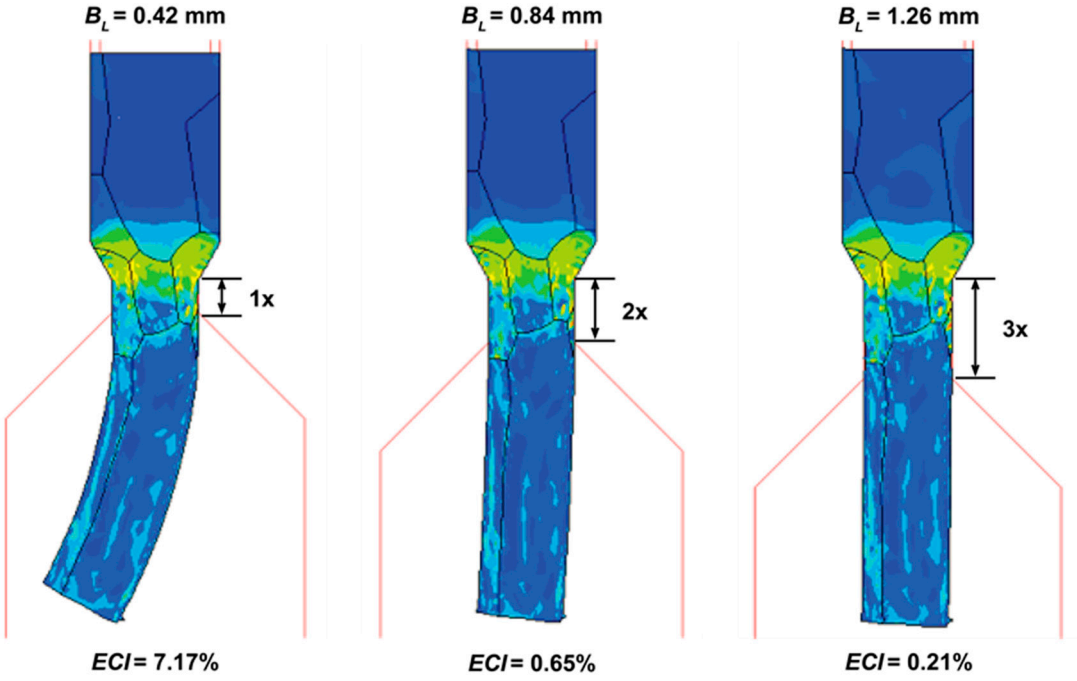

Figure 21. The results comparison among different bearing lengths.

Based on the results, the following observations and analysis could be made:

- For single-grain conditions (G_R = 0.75), if the grain sizes and grain boundaries were symmetric along the extrusion direction, the grain orientation was the dominating factor for the curvature. If the grain sizes and grain boundaries were not symmetric along the extrusion direction, the grain boundary at the high strain and die opening area was the dominating factor for the curvature. The interactive influences of the grain boundary and grain orientation also affected the curvature.
- For poly-grain conditions (G_R < 0.75), if the number of grains across the specimen increased up to 2.7, the curvature effects were dramatically reduced. The influences of the grain boundaries and grain orientations were not significant.
- For all conditions, if the bearing lengths (B_L) were extended beyond the exit diameter (D_E), the micro-extrusion pins were straightened.

Although this work was carried out by using the numerical simulation method, the findings of this research work fundamentally helped explain how the micro-extrusion parts were curved. Future work within this research would apply the FE techniques to the designed grain sizes and orientations under controlled micro-extrusion process parameters. Higher-grade aluminum alloys and multi-material extrusion would also be considered by using this same technique. The results of all the studies could be integrated in order to design and develop single-crystal parts by using the grain selector. The insights gained from this series of ongoing studies could be applied to the control and optimization of lightweight multi-material micro-parts.

4. Conclusions

This research work investigated the driving mechanism behind the curvature in the micro-extrusion of a 6063 aluminum alloy at room temperature. An FE simulation was used to observe the influences of the grain sizes, grain boundaries, grain orientations, and bearing lengths. The FE simulations were validated with experiments using a 66-μm grain-size billet, and the results agreed well. The billet grain

sizes were enlarged, ranging from poly-grain to single-grain conditions, and their material properties were extrapolated. The grain shapes (boundaries) were established, and the grain orientations were varied to determine the interactive effects on the curvature (Extrusion Curvature Index or ECI) of micro-extruded pins. The key finding was that the grain boundary was the dominating factor driving the mechanism of curvature in micro-extrusion under single-grain conditions.

Author Contributions: Conceptualization, N.M. and S.S.; Data curation, P.P. and N.M.; Formal analysis, P.P., N.M. and S.S.; Funding acquisition, N.M. and S.B.; Investigation, P.P. and N.M.; Methodology, P.P., N.M. and S.S.; Project administration, N.M.; Resources, N.M., T.F., N.T. and K.D.; Software, S.S.; Supervision, N.M., N.T., S.B. and K.D.; Validation, P.P. and T.F.; Visualization, N.M.; Writing—original draft, P.P.; Writing—review & editing, N.M. All authors have read and agreed to the published version of the manuscript.

Funding: This research was funded by the Thailand Research Fund (TRF), grant number MRG5980148. The APC was funded by Khon Kaen University.

Acknowledgments: The authors would like to acknowledge the supports of: LPN Metallurgical Research Center, Thailand, National Metal and Materials Technology Center (MTEC), Thailand; University of Toyama, Japan; Department of Mechanical Engineering, Northwestern University, USA; Department of Mechanical Engineering, Faculty of Engineering, Khon Kaen University; and Onward Giken Corporation, Japan.

Conflicts of Interest: The authors declare no conflict of interest.

References

1. Cullen, J.M.; Allwood, J.M. Mapping the Global Flow of Aluminum: From Liquid Aluminum to End-Use Goods. *Environ. Sci. Technol.* **2013**, *47*, 3057–3064. [CrossRef] [PubMed]
2. Alting, L.; Kimura, F.; Hansen, H.N.; Bissacco, G. Micro Engineering. *CIRP Ann.* **2003**, *52*, 635–657. [CrossRef]
3. Dong, X.; Chen, F.; Chen, S.; Liu, Y.; Huang, Z.; Chen, H.; Feng, S.; Zhao, L.; Wu, Z.; Zhang, X. Microstructure and microhardness of hot extruded 7075 aluminum alloy micro-gear. *J. Mater. Process. Technol.* **2015**, *219*, 199–208. [CrossRef]
4. Cowley, A.; Woodward, B. A Healthy Future: Platinum in Medical Applications. *Platin. Met. Rev.* **2011**, *55*, 98–107. [CrossRef]
5. Geiger, M.; Kleiner, M.; Eckstein, R.; Tiesler, N.; Engel, U. Microforming. *CIRP Ann.* **2001**, *50*, 445–462. [CrossRef]
6. Qin, Y. Micro-forming and miniature manufacturing systems—Development needs and perspectives. *J. Mater. Process. Technol.* **2006**, *177*, 8–18. [CrossRef]
7. Gronostajski, Z.; Pater, Z.; Madej, L.; Gontarz, A.; Lisiecki, L.; Łukaszek-Sołek, A.; Łuksza, J.; Mróz, S.; Muskalski, Z.; Muzykiewicz, W.; et al. Recent development trends in metal forming. *Arch. Civ. Mech. Eng.* **2019**, *19*, 898–941. [CrossRef]
8. Jeswiet, J.; Geiger, M.; Engel, U.; Kleiner, M.; Schikorra, M.; Duflou, J.; Neugebauer, R.; Bariani, P.; Bruschi, S. Metal forming progress since 2000. *CIRP J. Manuf. Sci. Technol.* **2008**, *1*, 2–17. [CrossRef]
9. Parasız, S.A.; Kinsey, B.L.; Mahayatsanun, N.; Cao, J. Effect of specimen size and grain size on deformation in microextrusion. *J. Manuf. Process.* **2011**, *13*, 153–159. [CrossRef]
10. Rosochowski, A.; Presz, W.; Olejnik, L.; Richert, M. Micro-extrusion of ultra-fine grained aluminium. *Int. J. Adv. Manuf. Technol.* **2007**, *33*, 137–146. [CrossRef]
11. Fann, K.-J.; Chen, C.-C. Grain Size in Aluminum Alloy 6061 under Hot Ring Compression Test and after T6 Temper. *Appl. Sci.* **2017**, *7*, 372. [CrossRef]
12. Justinger, H.; Hirt, G. Estimation of grain size and grain orientation influence in microforming processes by Taylor factor considerations. *J. Mater. Process. Technol.* **2009**, *209*, 2111–2121. [CrossRef]
13. Hansen, N. The effect of grain size and strain on the tensile flow stress of aluminium at room temperature. *Acta Metall.* **1977**, *25*, 863–869. [CrossRef]
14. Li, Y.; Bushby, A.J.; Dunstan, D.J. The Hall–Petch effect as a manifestation of the general size effect. *Proc. R. Soc. A Math. Phys. Eng. Sci.* **2016**, *472*, 20150890. [CrossRef]
15. Kim, G.-Y.; Ni, J.; Koç, M. Modeling of the Size Effects on the Behavior of Metals in Microscale Deformation Processes. *J. Manuf. Sci. Eng.* **2006**, *129*, 470–476. [CrossRef]
16. Wang, C.-J.; Guo, B.; Shan, D.-B.; Sun, L.-N. Effects of specimen size on flow stress of micro rod specimen. *Trans. Nonferrous Met. Soc. China* **2009**, *19*, s511–s515. [CrossRef]

17. Parasiz, S.A.; Kinsey, B.; Krishnan, N.; Cao, J.; Li, M. Investigation of Deformation Size Effects During Microextrusion. *J. Manuf. Sci. Eng.* **2006**, *129*, 690–697. [CrossRef]
18. Engel, U. Tribology in microforming. *Wear* **2006**, *260*, 265–273. [CrossRef]
19. Krishnan, N.; Cao, J.; Dohda, K. Study of the Size Effect on Friction Conditions in Microextrusion—Part I: Microextrusion Experiments and Analysis. *J. Manuf. Sci. Eng.* **2006**, *129*, 669–676. [CrossRef]
20. Mori, L.F.; Krishnan, N.; Cao, J.; Espinosa, H.D. Study of the Size Effects and Friction Conditions in Microextrusion—Part II: Size Effect in Dynamic Friction for Brass-Steel Pairs. *J. Manuf. Sci. Eng.* **2007**, *129*, 677–689. [CrossRef]
21. Vollertsen, F.; Biermann, D.; Hansen, H.N.; Jawahir, I.S.; Kuzman, K. Size effects in manufacturing of metallic components. *CIRP Ann.* **2009**, *58*, 566–587. [CrossRef]
22. Chan, W.L.; Fu, M.W.; Yang, B. Study of size effect in micro-extrusion process of pure copper. *Mater. Des.* **2011**, *32*, 3772–3782. [CrossRef]
23. Deng, J.H.; Fu, M.W.; Chan, W.L. Size effect on material surface deformation behavior in micro-forming process. *Mater. Sci. Eng. A* **2011**, *528*, 4799–4806. [CrossRef]
24. Lin, J.-F.; Li, F.; Zhang, J.-F. A new approach to investigate real flow stress in micro-extrusion. *Trans. Nonferrous Met. Soc. China* **2012**, *22*, s232–s238. [CrossRef]
25. Xinyun, W.; Mao, Z.; Na, T.; Ning, L.; Lin, L.; Jianjun, L. A Forming Load Prediction Model in BMG Micro Backward Extrusion Process Considering Size Effect. *Phys. Proced.* **2013**, *48*, 146–151. [CrossRef]
26. Ghassemali, E.; Tan, M.-J.; Wah, C.B.; Jarfors, A.E.W.; Lim, S.C.V. Grain size and workpiece dimension effects on material flow in an open-die micro-forging/extrusion process. *Mater. Sci. Eng. A* **2013**, *582*, 379–388. [CrossRef]
27. Ghassemali, E.; Tan, M.-J.; Jarfors, A.E.W.; Lim, S.C.V. Optimization of axisymmetric open-die micro-forging/extrusion processes: An upper bound approach. *Int. J. Mech. Sci.* **2013**, *71*, 58–67. [CrossRef]
28. Ghassemali, E.; Tan, M.-J.; Wah, C.B.; Lim, S.C.V.; Jarfors, A.E.W. Effect of cold-work on the Hall–Petch breakdown in copper based micro-components. *Mech. Mater.* **2015**, *80*, 124–135. [CrossRef]
29. Rajenthirakumar, D.; Sridhar, R.; Abenethiri, R.; Kartik, R.; Bagri, D. Experimental investigations of grain size effects in forward microextrusion. *Int. J. Adv. Manuf. Technol.* **2016**, *85*, 2257–2264. [CrossRef]
30. Wang, C.; Wang, C.; Xu, J.; Zhang, P.; Shan, D.; Guo, B. Interactive effect of microstructure and cavity dimension on filling behavior in micro coining of pure nickel. *Sci. Rep.* **2016**, *6*, 23895. [CrossRef] [PubMed]
31. Zhou, W.; Lin, J.; Dean, T.A.; Wang, L. A novel application of sideways extrusion to produce curved aluminium profiles: Feasibility study. *Procedia Eng.* **2017**, *207*, 2304–2309. [CrossRef]
32. Zhou, W.; Lin, J.; Dean, T.A.; Wang, L. Feasibility studies of a novel extrusion process for curved profiles: Experimentation and modelling. *Int. J. Mach. Tools Manuf.* **2018**, *126*, 27–43. [CrossRef]
33. Zhang, B.; Dodaran, M.; Ahmed, S.; Shao, S.; Meng, W.J.; Juul, K.J.; Nielsen, K.L. Grain-size affected mechanical response and deformation behavior in microscale reverse extrusion. *Materialia* **2019**, *6*, 100272. [CrossRef]
34. Truong, T.-T.; Hsu, Q.-C.; Tong, V.-C. Effects of Solid Die Types in Complex and Large-Scale Aluminum Profile Extrusion. *Appl. Sci.* **2020**, *10*, 263. [CrossRef]
35. Ye, T.; Li, L.; Guo, P.; Xiao, G.; Chen, Z. Effect of aging treatment on the microstructure and flow behavior of 6063 aluminum alloy compressed over a wide range of strain rate. *Int. J. Impact Eng.* **2016**, *90*, 72–80. [CrossRef]
36. Roters, F.; Eisenlohr, P.; Bieler, T.R.; Raabe, D. *Crystal Plasticity Finite Element Methods: In Materials Science and Engineering*; Wiley-VCH: Weinheim, Germany, 2011.
37. Funazuka, T.; Takatsuji, N.; Dohda, K.; Aizawa, T. Effect of Grain Size on Formability in Micro-extrusion-Research on Forward-Backward Micro-extrusion of Aluminum Alloy 1st Report-. *J. Jpn. Soc. Technol. Plast.* **2018**, *59*, 8–13. [CrossRef]
38. Pan, D.; Xu, Q.; Liu, B.; Li, J.; Yuan, H.; Jin, H. Modeling of grain selection during directional solidification of single crystal superalloy turbine blade castings. *JOM* **2010**, *62*, 30–34. [CrossRef]
39. Dai, H.J.; D'Souza, N.; Dong, H.B. Grain Selection in Spiral Selectors During Investment Casting of Single-Crystal Turbine Blades: Part I. Experimental Investigation. *Metall. Mater. Trans. A* **2011**, *42*, 3430–3438. [CrossRef]

40. Dai, H.J.; Dong, H.B.; D'Souza, N.; Gebelin, J.C.; Reed, R.C. Grain Selection in Spiral Selectors During Investment Casting of Single-Crystal Components: Part II. Numerical Modeling. *Metall. Mater. Trans. A* **2011**, *42*, 3439–3446. [CrossRef]
41. Zhang, H.; Xu, Q. Simulation and Experimental Studies on Grain Selection and Structure Design of the Spiral Selector for Casting Single Crystal Ni-Based Superalloy. *Materials* **2017**, *10*, 1236. [CrossRef]

Journal:	Coatings
Journal Impact Factor:	2.436
Paper Title:	Effects of Tool Coatings on Energy Consumption in Micro-Extrusion of Aluminum Alloy 6063
DOI:	10.3390/coatings10040381

coatings

MDPI

Article

Effects of Tool Coatings on Energy Consumption in Micro-Extrusion of Aluminum Alloy 6063

Sedthawatt Sucharitpwatskul [1], Numpon Mahayotsanun [1,*], Sujin Bureerat [1] and Kuniaki Dohda [2]

[1] Department of Mechanical Engineering, Faculty of Engineering, Khon Kaen University, 123 Moo 16 Mittraphap Rd., Nai-Muang, Muang 40002, Thailand; sedthaws@mtec.or.th (S.S.); sujbur@kku.ac.th (S.B.)

[2] Department of Mechanical Engineering, Northwestern University, 2145 Sheridan Road, Evanston, IL 60208, USA; dohda.kuni@northwestern.edu

* Correspondence: numpon@kku.ac.th

Received: 31 March 2020; Accepted: 11 April 2020; Published: 13 April 2020

Abstract: The tool wear rate and energy consumption were typically unknown in micro-extrusion, which made it difficult to optimize the tool design for both the final part quality and production cost. This study investigated the effects of tool coatings on energy consumption in the micro-extrusion of aluminum alloy 6063. Three main factors were considered in this study: (1) tool coating types, (2) bearing length, and (3) extrusion ratio. The micro-extrusion finite element simulation model was developed and validated with the micro-extrusion experiment. The results showed that increasing bearing lengths led to the increase in tool wear rate and energy consumption for all the coating types. The decreasing coefficient of friction values of the tool-billet interface led to a decrease in energy consumption. High hardness values of the tool surface and low bearing lengths helped increase tool life. Low values of coefficient of friction and bearing lengths helped decrease energy consumption.

Keywords: coating; energy consumption; finite element analysis; micro-extrusion

1. Introduction

Global demands in aluminum consumption have been rising, particularly in the areas that need lightweight [1]. New products, solutions, and processes must be developed in order to meet such high demands. Aluminum extrusion is one of the vital metal forming processes that provide net-shape and mass-production benefits [2]. The recent trend in miniaturization has shown that metallic micro parts (mechanical micro connector pins, miniature contact springs, and electronic parts with micro features) are growing in automobiles and electronics [3]. Micro-biomedical parts ranging from rod, wire, ribbon, and tube drawing, to sheet and foil manufacture, and highly precise screw machining are also commercially available [4]. One of the possible technologies to produce these metallic parts is micro forming [5]. The micro-extrusion process can be utilized to produce high precision miniaturized parts to add higher value to aluminum extrusion products [5–7]. Besides, increased strengths of micro-parts can also be achieved by using micro-extrusion [8–14].

Tribology heavily plays an essential role in micro-extrusion due to the increase in surface areas in comparison to the part dimensions [15,16]. Typical friction tests used in macro-extrusion might no longer be practical in the micro-scale [17,18]. To successfully characterize tribological behaviors in micro-extrusion, friction tests that can simulate the real forming conditions should be considered [19–21]. Fundamentally, an oxide layer formed on steel surface caused high friction, and the coefficient of friction was sensitive to the surface roughness during forming without lubrication [22]. Tool wear is apparent in extrusion due to the plastic deformation due to sliding [23,24]. Thus, different types of

tool coatings have been used to solve the wear problem [25,26]. For instance, in aluminum extrusion, AlCrN could be coated on the extrusion die (H13 material) [27]. Titanium coatings could also be applied to the steel surfaces [28].

Recently, Diamond-Like Carbon (DLC) has been applied in metal forming to reduce severe tool wear [29–32]. There have also been environmentally friendly multi-functional additives that can be applied to steel coating under severe mechanical, thermal, and chemical conditions [33]. Our previous work on applying different coatings to the micro forward-backward extrusion tools showed that DLC provided excellent tribological characteristics [34]. Based on our previous work on the Forward-Backward, Vertical, Slow-Speed Micro-Extrusion, we investigated the effects of tool geometry (die angle) and coating types (CrN, TiN, and DLC-PVD). However, there were the following factors that must be investigated further: (1) DLC-CVD, (2) high-speed extrusion, and (3) bearing length. In addition, the aspects of tool wear and energy consumption must be considered to optimize the production cost. Energy consumption is one of the crucial factors in micro-extrusion since it is directly related to cost and environmental impact [35]. Although extrusion of micro-scale products seems to consume minimal energy, producing these tiny parts in mass-production could be a great concern. Since experimental investigation on effects of tribology in micro-extrusion is difficult to setup and critical parameters are not easily measured, finite element simulation has been commonly used to analyze the forming and tribological behaviors in micro-extrusion [36].

The objective of this paper was to investigate the effects of tool coatings used in micro-extrusion to energy consumption. Various tool coatings were considered in this study. Finite element simulation was carried out to predict the energy consumption. The novelty of this was the investigation of wear rate and energy consumption of the considered tool coatings in an extrusion cycle. The obtained results and the information regarding the actual coatings development costs would provide the micro-manufacturing community the tool design guidelines in micro-extrusion.

2. Materials and Methods

2.1. Micro-Extrusion Experiment

The micro-extrusion machine used in this study is shown in Figure 1, which consists of actuator and extrusion assembly. The punch and dies are located in the extrusion assembly, as shown. The actuator could provide up to 19 kN force, 230 mm/s speed, and 30 mm stroke length. During the extrusion operation, a prepared billet was placed in the cavity of the dies. The punch was then moved to push the billet into the die cavity, extruding the billet into a smaller part. The experiments were carried out at room temperature with a ram speed of 100 mm/s and a forming stroke of 3.0 mm.

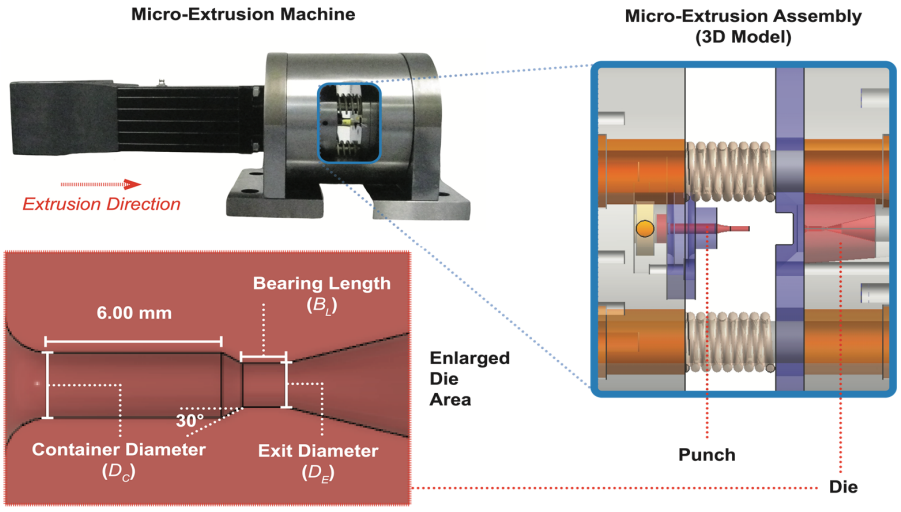

Figure 1. Micro-extrusion machine and components.

2.2. Materials

The billet material under investigation was 6063 aluminum alloy. The specimen billets were fabricated to have 1.7 mm in diameter and 6 mm in length by hot extrusion and machining. The non-annealed billets had a microstructure having approximately 64 μm grain size and a hardness value of 31 HV. The grain size of the billet material was measured by using the standard ASTM E112 [37]. The purpose of measuring the grain size was to quantitatively measure the average number of grains across the billet diameter. Since the investigated grain size was 64 μm, the average number of grains was approximately 27, which should provide homogeneous material property. As a result, the selected material model for the finite element was the power-law. The material model of the billet material was obtained, as shown in Equation (1).

$$\sigma = (168.4 \text{ MPa}) \cdot \varepsilon^{0.3} \quad (1)$$

where σ is the flow stress, and ε is the true strain. The punch and die materials were SKD11. The lubricant having 2.606 mm^2/s kinematic viscosity was applied between the die cavity and prepared billet before extrusion.

2.3. Considered Factors

The main factors investigated in this study were: (1) tool coating types, (2) bearing length (B_L), and (3) extrusion ratio (ER), as illustrated in Figure 2 and Tables 1–3.

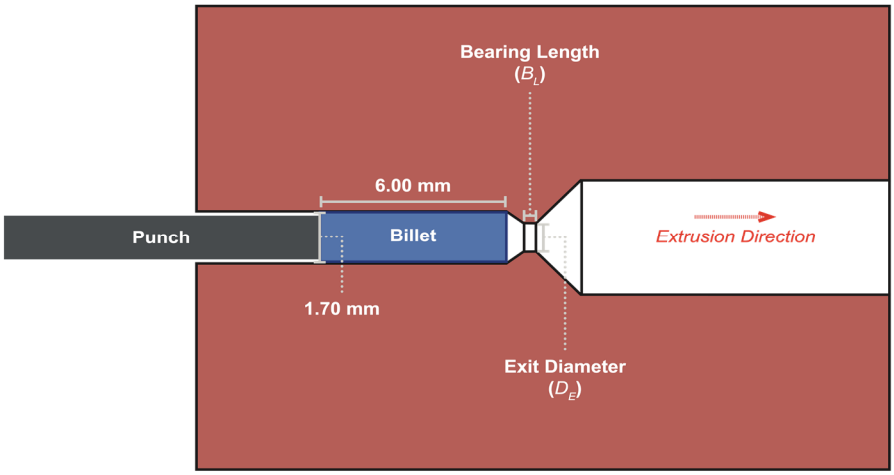

Figure 2. Schematic of micro-extrusion die and considered factors.

Table 1. Considered tool coatings in this study.

Parameters	CrN	TiN	DLC-CVD	DLC-PVD
Coating Hardness (HV)	1700	2100	4000	7000
Coating Thickness (μm)	2.0	1.0	1.0	0.7
Coefficient of Friction (COF)	0.45	0.55	0.11	0.11

Table 2. Considered bearing length (B_L) values in this study.

Parameters	Level 1 (Initial)	Level 2 (Low)	Level 3 (Medium)	Level 4 (High)
Bearing Length (B_L)	0.50 mm	1.00 mm	2.50 mm	3.00 mm

Table 3. Considered extrusion ratio (*ER*) values in this study.

Parameters	Level 1 (Low)	Level 2 (High)
Exit Diameter (D_E)	1.09 mm	0.55 mm
Extrusion Ratio (*ER*)	2.43	9.55

The tool coatings were developed and manufactured by Onward Giken Co. (Ishikawa, Japan). Chromium Nitride (CrN), Titanium Nitride (TiN), Diamond-Like Carbon (DLC) were commonly applied to tool coatings in severe forming applications. Note that DLC-CVD was the DLC coating produced by using Chemical Vapor Deposition (CVD). DLC-PVD was the DLC coating produced by using Physical Vapor Deposition (PVD). The coating properties were specific for this study only. The coating hardness values were measured by Vickers Hardness Testing. The coating thickness measurement was carried out by using the microscope. Note that the difference in coating thickness values was due to the available coating options provided by Onward Giken Corporation, Japan. The coefficient of friction values was obtained from the ball-on-disc test.

The extrusion ratio (*ER*) could be calculated from Equation (2).

$$ER = (\pi/4) \cdot (D_C{}^2/D_E{}^2) \quad (2)$$

where D_C is the container diameter, and D_E is the exit diameter. Note that the container diameter (D_C) used in this study was constant (1.70 mm), and the exit diameters (D_E) were varied to obtain different *ER* values.

2.4. Finite Element Simulation

The Lagrangian finite element code MSC.Marc 2017 was used to investigate the considered factors, as illustrated in Figure 3. The following assumptions were made: (1) 2D axisymmetric conditions, (2) no heat transfer to the tools, and (3) using the power-law material model. An axisymmetric model was set up to simulate the extrusion process. The 4-node fully integration element was used, resulting in 2040 elements. The tools (punch, container, die bearing, and die relief) were designated as rigid bodies. The initial diameter of the cylinder billet was 1.7 mm, and its length was 6 mm. In order to accurately describe the interface condition between billet and tooling, three friction models were evaluated.

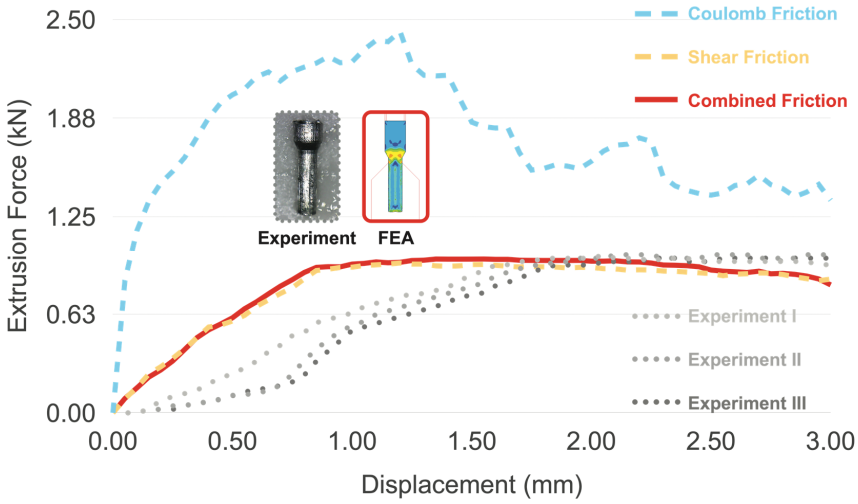

Figure 3. Comparison between considered friction models with the micro-extrusion experiment.

2.4.1. Coulomb Friction Model

This is an approximate model to calculate the friction force, resisting the relative lateral motion of two solid surfaces in contact. The two regimes of friction are static friction between non-moving surfaces. The governing equation is shown in Equation (3).

$$f = \mu_s N \tag{3}$$

where f is friction force, μ_s is the static friction coefficient, and N is the normal load. The Coulomb friction force (f) may take any value from zero up to $\mu_s N$, and the direction of the frictional force against a surface is opposite to the motion that the surface would experience in the absence of friction.

2.4.2. Shear Friction Model

Shear friction model, which relates the friction stress to the shear strength of the deformed material. This model uses shear flow stress to replace friction stress when friction stress is greater than the shear strength of the deformed material. When the friction stress is lower than the shear strength of the deformed material, the friction stress follows the Coulomb friction law. The shear friction model can be written, as shown in Equation (4).

$$f = k \text{ when} \geq \mu_s N \tag{4}$$

where k is the shear friction force.

2.4.3. Combined Friction Model

The Coulomb friction law is typically used in combination with limiting stress when the friction stress is lower than the shear strength of the deformed material. When the calculated friction stress is greater than the shear strength of the deformed material, shear flow stress is used to replace the friction stress. This model was also applied in the micro-forming process carried out by Ghassemali et al. [38]. The governing equation of this model is shown in Equation (5).

$$f = \mu_s N, \text{ when } \mu_s N < k; f = k \text{ when } \mu_s N \geq k \tag{5}$$

The coefficient of friction values used in this study was varied based on the considered tool coatings.

The main purpose of this study was to determine precisely how each considered coating could reduce wear and consume energy in one extrusion cycle. The finite element model was validated with three experiments (one extrusion cycle each). In the validation condition, the billet was extruded from 1.70 mm to 1.09 mm with 100 mm/s speed and 2 mm stroke. The coating used in the validation condition was DLC-PVD. The same trend could be observed on the other considered coatings. The simulation results were compared with those of the experiment, as illustrated in Figure 3. The extrusion forces of both simulation and experiment were plotted against the extrusion stroke. The Coulomb friction model provided the highest extrusion force. Both shear friction and combined friction had similar values of extrusion forces, lower than those of the Coulomb friction model. Based on the observation of forming behaviors of micro-extrusion experiments, the Coulomb friction model tended to overestimate the friction stress, particularly under high contact pressures. When the friction stress was greater than the shear strength of the deformed material, shear flow stress should be used to replace the friction stress. Nevertheless, when the friction stress was lower than the shear strength of the deformed material, the friction stress should follow the Coulomb friction model. As a result, the combined friction model was selected in order to represent the tool-billet interface in this study.

The wear rate and energy consumption of one extrusion cycle were critical for our study due to the following reasons:

(1) The wear rate per cycle would be used to predict the number of cycles prior to tool wear (coating thickness depletion). Thus, the final part geometry could be precisely controlled, and the tool could be adequately maintained, lowering the production cost.
(2) The energy consumption per extrusion cycle would be used to predict the energy cost by using each considered tool coating. Each extrusion energy cycle would be multiplied by the predicted number of cycles from (1) to obtain the total energy consumption.

Both of the calculated values from (1), (2), and the actual coatings development costs would provide the tool design guidelines for the micro-extrusion engineers.

After the finite element simulation model was validated, the considered factors shown in Tables 1–3 were used as the input parameters to the finite element simulation. The tool wear rate was also investigated in this study by using Archard's equation, as shown in Equation (6).

$$W = K \times F \times Gt/H \tag{6}$$

where W is tool wear, K is the wear coefficient ($K = 1 \times 10^{-12}$ in this study), F is the normal load, Gt is the sliding distance, and H is the hardness of the worn material (Table 1). In order to evaluate the tool wear rate (W_r), the above equation could also be written in Equation (7).

$$Wr = K \times \sigma \times V/H \tag{7}$$

where σ is the normal stress, and V is the relative velocity, which is 100 mm/s in this study.

In order to evaluate the effects of tool coatings on energy consumption (E), the extrusion forces (F) obtained from each testing condition were multiplied by the extrusion stroke (S), as shown in Equation (8).

$$E = F \times S \tag{8}$$

Since only one extrusion cycle was compared for all the testing conditions, tool wear rate and extrusion energy would be considered only for one cycle as well.

3. Results

The comparison of tool wear rates among the considered tool coatings is illustrated in Figure 4. Note that these were the comparison results from the simulations. In addition, the left figure ($ER = 2.43$) was the enlarged section of tool wear rate of the right figure ($ER = 9.55$). According to the figure, the tool wear rate of all the coatings increased with bearing length and extrusion ratio. This was due to the fact that higher bearing length increased the sliding lengths between the billet and the tools, causing the tool wear rate to increase. High extrusion ratio also implied that the forces required to plastically deform the billet into the die increased, causing higher stresses to the tools; thus, tool wear rate increased. At both extrusion ratios, increasing bearing length from 0.5 mm to 3.0 mm would increase the tool wear rate of approximately 40%. This phenomenon should be noted because extrusion engineers tend to increase bearing lengths in order to balance the material flow without realizing that a slight increase in bearing lengths could shorten tool life dramatically. Since the tool wear rate was inversely proportional to the tool hardness, the highest to lowest tool wear rate values range from CrN, TiN, DLC-CVD, and DLC-PVD, respectively. If the tool wear rates between DLC-CVD and DLC-PVD were compared, DLC-PVD provided lower tool wear rates than DLC-CVD did. This was mainly due to the fact that DLC-PVD had higher coating hardness value. Since the tool-billet interfaces of both DLC-CVD and DLC-PVD had the same coefficient of friction, the higher hardness value of DLC-PVD played an important role in lowering the tool wear rats. As a result, coatings that provided high hardness values would generally provide longer tool life. Nevertheless, the hardness values used in this study were mainly the hardness values of the tool surface (coated thickness shown in Table 1). One should be concerned that the bulk hardness values of the tool should not be too high, which would easily cause tool breakage.

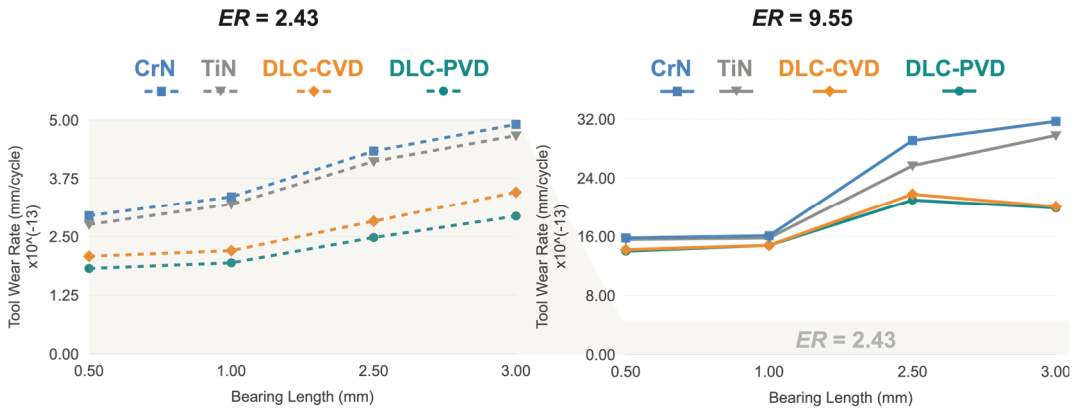

Figure 4. Comparison of tool wear rates among the considered tool coatings.

The comparison of energy consumptions among the considered tool coatings is displayed in Figure 5. Note that these were the comparison results from the simulations. In addition, the left figure (*ER* = 2.43) was the enlarged section of tool wear rate of the right figure (*ER* = 9.55). According to the figure, extrusion energy was increased with increasing bearing lengths and extrusion ratios. This was explained by the fact that increasing bearing lengths and extrusion ratios simply required more extrusion forces to overcome friction and plastic deformation during extrusion. Higher friction coefficients of the tool-billet interface provide higher friction values, extrusion forces, and extrusion energy values. It could be observed that both DLC-CVD and DLC-PVD had the same coefficient of friction values, thus, giving the same (lowest) energy consumption values. In addition, reducing the coefficient of friction values from 0.45 to 0.11 could cause energy consumption to drop approximately 50%. It should also be noted that increasing bearing lengths from 0.5 mm to 3.0 mm could cause energy consumption to rise from 10% to 30% for both extrusion ratios.

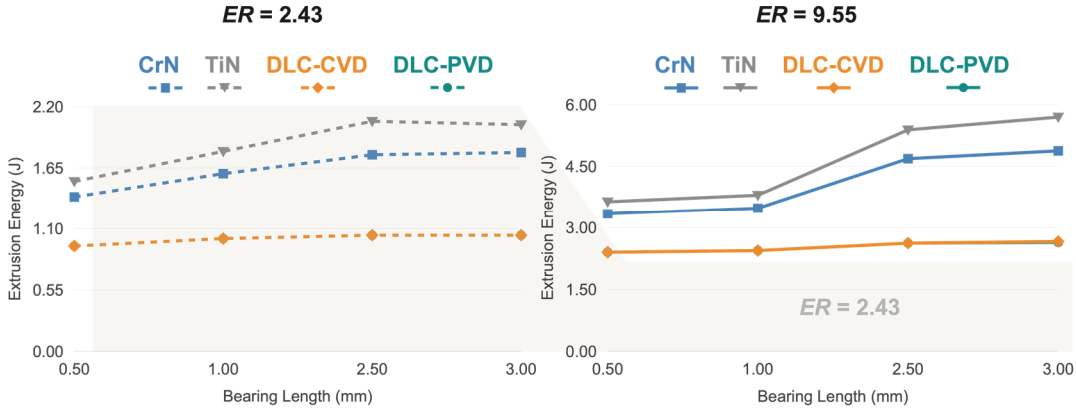

Figure 5. Comparison of energy consumptions among the considered tool coatings.

Although extrusion ratios significantly affected both tool life and energy consumption, modern extrusion profiles typically had high extrusion ratios and could not be avoided. As a result, extrusion engineers should pay attention to hardness values of the tool surface and bearing lengths if tool life was a concern. If energy consumption was a concern, bearing lengths and coefficient of friction of tool-billet interface should be paid attention to.

4. Discussion

The obtained results from the previous section showed that the DLC coatings (DLC-CVD and DLC-PVD) provided low tool wear rates, which agreed with many other forming processes on steel-aluminum interfaces [39]. The results demonstrated that DLC coated tools would be strong

candidates for friction and wear reduction, particularly in the micro-extrusion process at a high strain rate. Nevertheless, the DLC-PVD coating had a higher hardness value than that of DLC-CVD in this study. Thus, the lowest tool wear rate could be obtained by using DLC-PVD. In addition, both DLC-CVD and DLC-PVD provided the lowest energy consumption, which would make DLC-PVD more preferable due to its lower tool wear rate. Nevertheless, the bearing length should be kept minimum in order to keep both the tool wear rate and energy consumption low. The understanding of the interactive effects was crucial for extrusion engineers to select proper tool coatings for the micro-extrusion process to achieve optimal production.

For the future research outlook based on the results of this study, higher-grade alloys should be considered due to their increased demands in the automotive and aerospace applications. The other lightweight materials should also be investigated, particularly for biomedical product development. The more challenging studies would involve much higher extrusion ratio (*ER*) and complex-shape profiles in the micro-scale. Not only would the difficulty lie in the deformation, but the real challenge would also be in the development of high tribological performance and low-cost tool coatings.

5. Conclusions

The effects of tool coatings on energy consumption in micro-extrusion of 6063 aluminum alloy were investigated. Three main factors were considered: tool coating types, bearing length (B_L), and extrusion ratio (*ER*). The finite element simulation model was set up and validated with the micro-extrusion experiment. The tool wear rate and extrusion energy were calculated. The significant findings of the study could be summarized as follows:

(1) Increasing bearing lengths from 0.5 mm to 3.0 mm led to the increase in tool wear rate of 40% and energy consumption of 10%–30% for all the coating types.
(2) Reducing the coefficient of frictions from 0.45 to 0.11 led to a decrease in energy consumption of 50%.
(3) High hardness values of the tool surface and low bearing lengths are critical to tool life extension.
(4) Low coefficient of friction values of the tool-billet interface and low bearing lengths are critical to energy consumption.

Author Contributions: Conceptualization, N.M.; data curation, S.S.; formal analysis, S.S. and N.M.; funding acquisition, N.M.; investigation, N.M.; methodology, N.M.; project administration, N.M.; resources, N.M.; software, S.S.; supervision, N.M., S.B., and K.D.; validation, N.M.; visualization, N.M.; writing—original draft, S.S.; writing—review and editing, N.M. All authors have read and agreed to the published version of the manuscript.

Funding: This research was funded by the THAILAND RESEARCH FUND (TRF), grant N MRG5980148, and the APC was funded by Khon Kaen University (KKU), Muang, Thailand.

Acknowledgments: The authors would like to acknowledge the supports of National Metal and Materials Technology Center (MTEC), Khlong Nueng, Thailand, University of Toyama, Toyama, Japan, Department of Mechanical Engineering, Northwestern University, Evanston, IL, USA, Department of Mechanical Engineering, Faculty of Engineering, Khon Kaen University, Muang, Thailand and Onward Giken Corporation, Tokyo, Japan.

Conflicts of Interest: The authors declare no conflict of interest.

References

1. Cullen, M.; Allwood, J. Mapping the global flow of aluminum: From liquid aluminum to end-use goods. *Environ. Sci. Technol.* **2013**, *47*, 3057–3064. [CrossRef] [PubMed]
2. Gronostajski, Z.; Pater, Z.; Madej, L.; Surdacki, P.; Lisiecki, L.; Lukaszek-Solek, A.; Łuksza, J.; Mróz, S.; Muskalski, Z.; Muzykiewicz, W.; et al. Recent development trends in metal forming. *Arch. Civ. Mech. Eng.* **2019**, *19*, 898–941. [CrossRef]
3. Alting, L.; Kimura, F.; Hansen, H.N.; Bissacco, G. Micro engineering. *CIRP Ann.* **2003**, *52*, 635–657. [CrossRef]
4. Cowley, A.; Woodward, B. A healthy future: Platinum in medical applications. *Platin. Metals Rev.* **2011**, *55*, 98–107. [CrossRef]

5. Vollertsen, F.; Friedrich, S.; Kuhfuß, B.; Maaß, P.; Thomy, C.; Zoch, H.-W. Micro forming processes. In *Cold Micro Metal Forming. Lecture Notes in Production Engineering*; Vollertsen, F., Friedrich, S., Kuhfuß, B., Maaß, P., Thomy, C., Zoch, H.W., Eds.; Springer: Cham, Switzerland, 2020.
6. Rosochowski, A.; Presz, W.; Olejnik, L.; Richert, M. Micro-extrusion of ultra-fine grained aluminium. *Int. J. Adv. Manuf. Technol.* **2007**, *33*, 137–146. [CrossRef]
7. Mahayotsanun, N.; Lee, H.C.; Cheng, T.J.; Chuang, Y.; Tu, K.Y.; Ehmann, K.; Cao, J. Development of the High-Speed Micro-Extrusion machine to investigate strain rate and size effects. In Proceedings of the 2009 International Conference of Micro-Manufacturing (4M/ICOMM 2009), Karlsruhe, Germany, 23–25 September 2009; pp. 383–386.
8. Kuhfuss, B. Bulk metal forming. In *Micro Metal Forming*; Springer: Berlin, Germany, 2013; pp. 103–133.
9. Li, Y.; Bushby, A.J.; Dunstan, D.J. The Hall–Petch effect as a manifestation of the general size effect. *Proc. R. Soc. A* **2016**, *472*, 20150890. [CrossRef] [PubMed]
10. Justinger, H.; Hirt, G. Estimation of grain size and grain orientation influence in microforming processes by Taylor factor considerations. *J. Manuf. Process.* **2011**, *13*, 153–159. [CrossRef]
11. Parasız, S.A.; Kinsey, B.L.; Mahayotsanun, N.; Cao, J. Effect of specimen size and grain size on deformation in microextrusion. *J. Manuf. Process.* **2009**, *209*, 2111–2121. [CrossRef]
12. Chan, W.L.; Fu, M.W.; Yang, B. Study of size effect in micro-extrusion process of pure copper. *Mater Des.* **2011**, *32*, 3772–3782. [CrossRef]
13. Fu, M.W.; Chan, W.L. Size effects in micro-scaled plastic deformation. In *Micro-scaled Products Development via Microforming*; Springer: London, UK, 2014; pp. 9–55.
14. Rajenthirakumar, D.; Sridhar, R.; Abenethiri, R.; Kartik, R.; Bagri, D. Experimental investigations of grain size effects in forward microextrusion. *Int. J. Adv. Manuf. Technol.* **2016**, *85*, 2257–2264. [CrossRef]
15. Wang, C.; Wang, C.; Xu, J.; Zhang, P.; Shan, D.; Gao, B. Interactive effect of microstructure and cavity dimension on filling behavior in micro coining of pure nickel. *Sci. Rep.* **2016**, *6*, 23895. [CrossRef] [PubMed]
16. Engel, U. Tribology in microforming. *Wear* **2006**, *260*, 265–273. [CrossRef]
17. Dixit, U.S.; Yadav, V.; Narayanan, G.R.; Bhardwaj, N. Friction in micromanufacturing. *J. Micromanufacturing* **2018**, *1*, 76–91. [CrossRef]
18. Yao, Z.; Mei, D.; Shen, H.; Chen, Z. A friction evaluation method based on barrel compression test. *Tribol. Lett.* **2013**, *51*, 525–535. [CrossRef]
19. Zhou, F.; Suh, C.-M.; Kim, S.-S.; Murakami, R.-I. Sliding-wear behavior of TiN- and CrN-coated 2024 aluminum alloy against an Al2O3 ball. *Tribol. Lett.* **2002**, *13*, 173–178. [CrossRef]
20. Eriksen, R.; Calaon, M.; Arentoft, M.; Bay, N. Benchmarking of direct and indirect friction tests in micro forming. *Key Eng. Mater.* **2012**, *504–506*, 581–586. [CrossRef]
21. Groche, P.; Muller, C.; Jahn, A. Effects of the tool lubrication in cold forging. *Tribol. Lett.* **2014**, *53*, 599–605. [CrossRef]
22. Groche, P.; Kramer, P.; Zang, Z.; Rezanov, V. Prediction of the evolution of the surface roughness in dependence of the lubrication system for cold forming processes. *Tribol. Lett.* **2015**, *59*, 1–9. [CrossRef]
23. Osakada, K.; Matsumoto, R. Fundamental study of dry metal forming with coated tools. *CIRP Ann. Manuf. Technol.* **2000**, *49*, 161–164. [CrossRef]
24. Biswas, S.K.; Singh, R.A. Wear of metals—Influence of some primary material properties. *Tribol. Lett.* **2002**, *13*, 203–207. [CrossRef]
25. Wang, S.Q.; Wei, M.X.; Wang, F.; Cui, X.H.; Dong, C. Transition of mild wear to severe wear in oxidative wear of H21 steel. *Tribol. Lett.* **2008**, *32*, 67–72. [CrossRef]
26. Prieske, M.; Hasselbruch, H.; Mehner, A.; Vollertsen, F. Friction and wear performance of different carbon coatings for use in dry aluminium forming processes. *Surf. Coat. Technol.* **2019**, *357*, 1048–1059. [CrossRef]
27. Hilda, R.; Bergsa, T.; Mattfelda, P.; Trautha, D.; Klockea, F.; Hoffmannb, D.C.; Kruppeb, N.C.; Brögelmannb, T.; Bobzinb, K. Analysis of wear phenomena during forward extrusion under dry friction conditions. *Wear* **2019**, *426–427*, 1362–1370. [CrossRef]
28. Ahmad, F.; Zhang, L.; Zheng, J.; Sidra, I.; Zhang, S. Characterization of AlCrN and AlCrON coatings deposited on plasma nitrided AISI H13 steels using ion-source-enhanced arc ion plating. *Coatings* **2020**, *10*, 306. [CrossRef]
29. Abrashov, A.; Grigoryan, N.; Vagramyan, T.; Asnis, N. On the mechanism of formation of conversion titanium-containing coatings. *Coatings* **2020**, *10*, 328. [CrossRef]

30. Wang, C.; Shan, D.; Guo, B. DLC-Coated tools for micro-forming. In *Micromanufacturing Engineering and Technology*, 2nd ed.; Qin, Y., Ed.; William Andrew: Amsterdam, The Netherlands, 2015; pp. 487–512.
31. Yang, M.; Shimizu, T.; Hu, J.; Shiratori, T. An integrated precise engineering for micro forming. *MATEC Web Conf.* **2018**, *190*, 01003. [CrossRef]
32. Evaristo, M.; Fernandes, F.; Cavaleiro, A. Room and high temperature tribological behaviour of W-DLC coatings produced by DCMS and hybrid DCMS-HiPIMS configuration. *Coatings* **2020**, *10*, 319. [CrossRef]
33. Kanda, K.; Suzuki, S.; Niibe, M.; Hasegawa, T.; Suzuki, T.; Saitoh, H. Local structure analysis on Si-containing DLC films based on the measurement of C K-Edge and Si K-Edge X-ray absorption spectra. *Coatings* **2020**, *10*, 330. [CrossRef]
34. Atta, A.M.; Ahmed, M.A.; Al-Lohedan, H.A.; El-Faham, A. Multi-Functional cardanol triazine schiff base polyimine additives for self-healing and super-hydrophobic epoxy of steel coating. *Coatings* **2020**, *10*, 327. [CrossRef]
35. Funazuka, T.; Takatsuji, N.; Dohda, K.; Mahayotosanun, N. Effect of Die angle and friction condition on formability in micro extrusion—Research on micro forward-backward extrusion of aluminum alloy 2nd report. *J. Jpn. Soc. Technol. Plast.* **2018**, *59*, 7–12.
36. Saboori, M.; Bakhshi-Jooybari, M.; Noorani-Azad, M.; Gorji, A. Experimental and numerical study of energy consumption in forward and backward rod extrusion. *J. Mater. Process. Technol.* **2006**, *177*, 612–616. [CrossRef]
37. Zhang, B.; Dodaran, M.; Ahmed, S.; Shao, S.; Meng, W.J.; Juul, K.J.; Nielsen, K.L. Grain-size affected mechanical response and deformation behavior in microscale reverse extrusion. *Materialia* **2019**, *6*, 100272. [CrossRef]
38. Ghassemali, E.; Tan, M.J.; Jarfors, A.E.W.; Lim, S.C.V. Progressive microforming process: Towards the mass production of micro-parts using sheet metal. *Int. J. Adv. Manuf. Technol.* **2012**, *66*, 5–8. [CrossRef]
39. Murakawa, M.; Takeuchi, S. Evaluation of tribological properties of DLC films used in sheet forming of aluminum sheet. *Surf. Coat. Technol.* **2003**, *163–164*, 561–565. [CrossRef]

Journal:	Key Engineering Materials
Journal Impact Factor:	0.350
Paper Title:	Effects of Friction Models, Geometry and Position of Tool on Curving Tendency of Micro-Extrusion 6063 Aluminum Alloy Pins
DOI:	10.4028/www.scientific.net/KEM.739.135

Effects of Friction Models, Geometry and Position of Tool on Curving Tendency of Micro-Extrusion 6063 Aluminum Alloy Pins

Sedthawatt Sucharitpwatskul[1,a], Numpon Mahayotsanun[1,b], Sasawat Mahabunphachai[2,c], Tatsuya Funazuka[3,d], Norio Takatsuji[3,e] and Kuniaki Dohda[4,f]

[1] Department of Mechanical Engineering, Faculty of Engineering, Khon Kaen University, Khon Kaen, 40002, Thailand

[2]National Metal and Materials Technology Center (MTEC), Thailand Science Park, Pathum Thani, 12120, Thailand

[3]Graduate School of Science and Engineering for Research, University of Toyama, Toyama, 930-8555, Japan

[4]Department of Mechanical Engineering, Northwestern University, Illinois, 60208 USA

[a]sedthaws@mtec.or.th, [b]numpon@kku.ac.th, [c]sasawatm@mtec.or.th, [d]d1571001@ems.u-toyama.ac.jp, [e]takatuji@eng.u-toyama.ac.jp, [f]dohda.kuni@northwestern.edu,

*Corresponding Author: numpon@kku.ac.th

Keywords: Alluminum Alloy; Curving; Finite Element Method; Friction; Geometry; Micro-Extrusion; Position.

Abstract. Micro-extrusion process is one of the micro-forming technology for fabrication of micro-parts such as micro-gear shaft for microelectromechanical system (MEMS) and micro pins for electronic parts. This paper presents the friction models effects and geometry effects on curving tendency of micro-extrusion 6063 aluminum alloy pins. Three friction models were considered: (1) Coulomb friction, (2) plastic shear friction, and (3) combined (Coulomb & plastic shear) friction. The finite element simulation was carried out and the results showed that the combined friction model accurately predicted the micro-extrusion results. Then, four tool geometry and position effects were investigated: (1) punch shift length, (2) die angle, (3) die shift length, and (4) bearing length. The finite element simulation was carried out to determine these tool geometry and position effects on the curving tendency of micro-extruded pins. The results showed that punch shift length and die angle did not affect the curving tendency. However, die shift length caused the micro-extruded pins to curve. The increase in bearing length helped straighten the micro-extruded pins.

Introduction

Micro-forming is one of the key technologies to produce net-shape micro parts [1-4] and micro-extrusion is one of the commonly used processes in micro-forming. Micro-extrusion allows high production rates, is suitable for mass production, produces near-net-shape components, and allows for 3-dimensional part geometry. One of the most concerned problems in micro-extrusion is the curving tendency of micro-extruded pins. Several studies have been carried out to explain the curving tendency in micro-extrusion [5-14]. The main conclusion from these research works is that grain (crystal) orientations are the major driving force of curved pins if the grain size is large comparable to the specimen size. The authors of this paper are concerned if tool geometry and position could contribute to the curving tendency of the micro-extruded pins. As a result, this paper aims to investigate the effects of tool geometry and position on the curving tendency in micro-extrusion by using finite element (FE) simulation. Since friction also plays an important role in forming behaviors, three friction models are considered in order to apply the most suitable friction model for micro-extrusion.

Micro-Extrusion Experiment

The forward-backward micro-extrusion was used in this study. Fig.1 showed a conical die had the container diameter of 1.71 mm and the bearing diameter of 1.09 mm. Chromium nitride (CrN) was coated on the die surface and the die had the average surface roughness (Ra) values of 0.05 μm. Fig. 2 showed the punch having diameter of 1.47 mm. The test material under investigation was 6063 aluminum alloy. The specimen billets were fabricated to have 1.7 mm in diameter and 6 mm in length by hot extrusion and machining. The non-annealed billets had a microstructure having approximately 46 μm grain size and hardness value of 50 HV. The material model of the test material is expressed as in Eq. 2.

$$\sigma = (265.3 \text{ MPa})\, \varepsilon^{0.27} \tag{2}$$

where σ is flow stress and ε is strain. During the extrusion, test pieces (billets) were inserted into the die and pushed to form micro-extruded pin. The experiments were carried out at room temperature with a ram speed of 0.1 mm/s and a forming stroke of 3.5 mm.

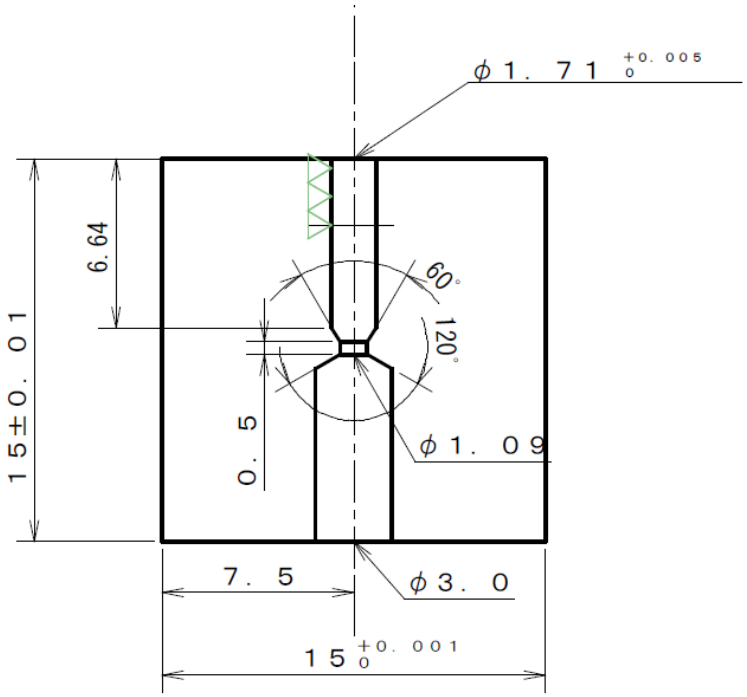

Fig. 1 Schematic of the micro-extrusion die (Units are in mm).

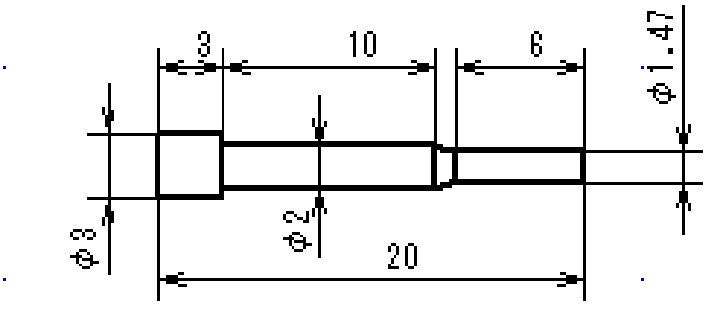

Fig. 2 Schematic of the micro-extrusion punch (Units are in mm).

Micro-Extrusion Simulation

The numerical studies of the suitable friction models for micro-extrusion were carried out in the Lagrangian finite element code MSC.Marc 2015. The micro-extrusion process was simplified with 2D axisymmetric analysis. The tools in the simulations were rigid. Note that the following assumptions were made:

(1) 2D axisymmetric conditions.

(2) No heat transfer to the tools.

(3) Using power law material model.

Considering the symmetry of the process, an axisymmetric model was set up to simulate the extrusion process. The 4-node fully integration element was used. Totally, 2,040 elements were generated. The punch, container, die angle, bearing, and relief were designated as rigid bodies. The initial diameter of the cylinder billet was 1.7 mm and its height was 6 mm. The diameter of the formed part was 1.09 mm. The interface regions were 4 pairs, namely, punch-billet interface, container-billet interface, die angle-billet interface, and die bearing-billet interface. Three friction models were used to describe the interface condition between billet and tooling.

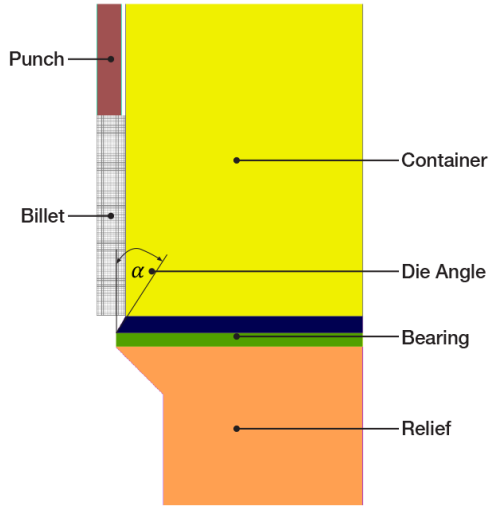

Fig. 3 FE setup of the micro-extrusion test.

(1) Coulomb friction model. The Coulomb friction resists relative lateral motion of two solid surfaces in contact. The two regimes of friction are static friction between non-moving surfaces. The coulomb friction is an approximate model used to calculate the friction force. It is governed by Eq. 3:

$$f \leq \mu_s N \tag{3}$$

where f is friction force, μ_s is static friction coefficient, and N is normal load. The Coulomb friction force f, may take any value from zero up to μN, and the direction of the frictional force against a surface is opposite to the motion that surface would experience in the absence of friction.

(2) Shear friction model. When the friction stress is lower than the shear strength of the deformed material, the friction stress follows the coulomb friction law. When the calculated friction stress is greater than the shear strength of the deformed material, shear flow stress is used to replace the friction stress. This is shown in Eq. 4:

$$f = k \text{ when } \mu_s N \geq k \tag{4}$$

where k is the shear friction force. The shear friction model relates the friction stress to the shear strength of the deformed material.

(3) Combined friction model. The Coulomb friction law is normally used in combination with a limiting stress when the friction stress is lower than the shear strength of the deformed material. When the calculated friction stress is greater than the shear strength of the deformed material, shear flow stress is used to replace the friction stress. This is shown in Eq. 5:

$$f = \mu_s N, \text{ when } \mu_s N < k \; ; \; f = k \text{ when } \mu_s N \geq k \tag{5}$$

The coefficient of friction was 0.45 and the interface friction factor was 0.26 for all the friction models.

Regarding the consideration of tool geometry and position effects, Fig. 4 and Fig. 5 demonstrate the schematic of the micro-extrusion parameters. Table 1 shows the considered tool geometry and position parameters in this study.

Table 1. Considered tool geometry and position parameters.

Parameters	Values
Punch shift length (P_s)	0 µm, 120 µm
Die angle (α)	30º, 60º, 90º
Die shift length (D_s)	0 µm, 100 µm
Bearing length (L_{br})	0.5 mm, 1.0 mm, 1.5 mm

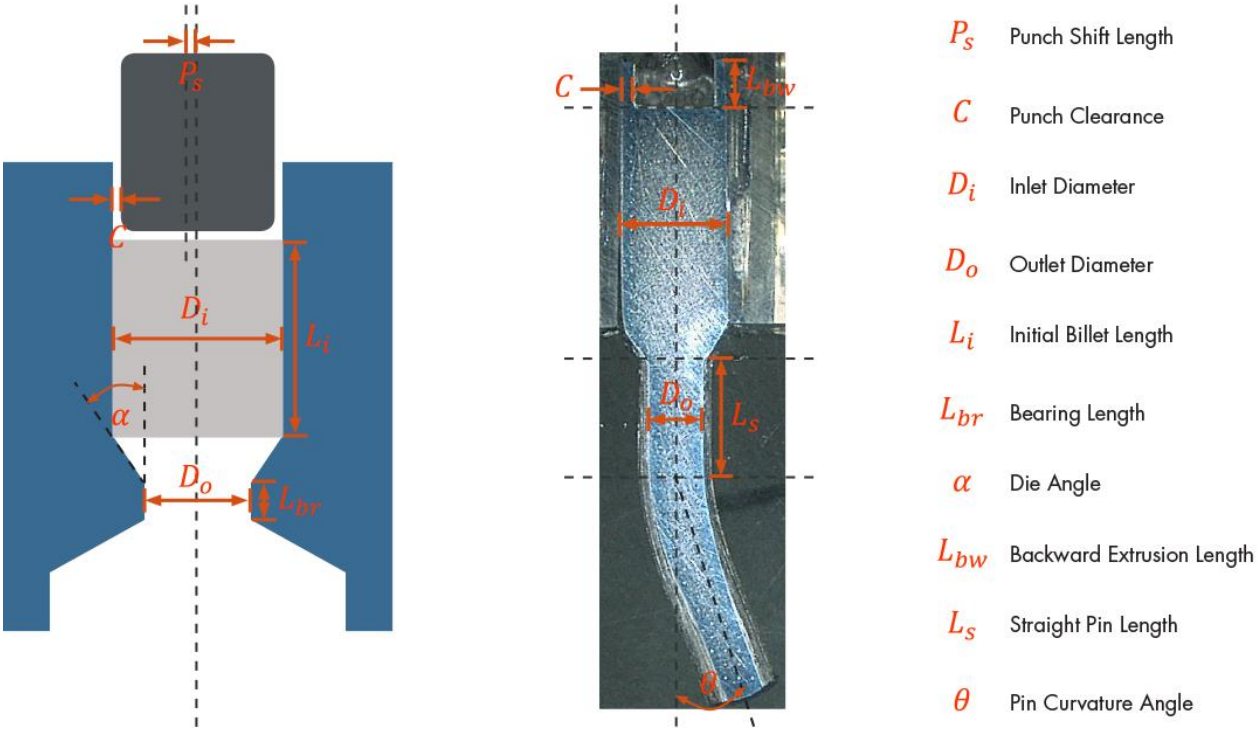

Fig. 4 Micro-extrusion parameters.

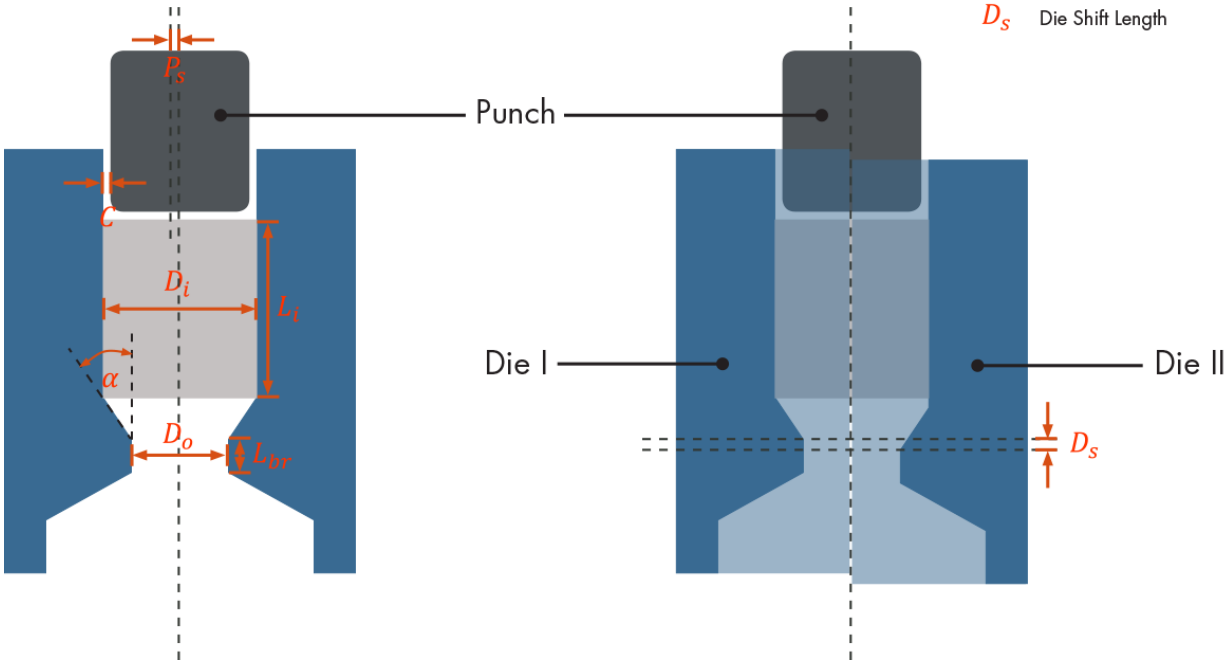

Fig. 5 Die shift parameter in micro-extrusion.

Results and Discussions

Fig. 6 shows the comparison of the simulated extrusion force and stroke curves of all friction interface conditions. The extrusion force of frictionless interface conditions is the lowest value among all friction interface conditions. The Coulomb friction model provides the highest extrusion force. Both shear friction and combined friction have similar values of extrusion forces, higher than those of frictionless model and lower than those of Coulomb friction model. Based on the observation of forming behaviors of micro-extrusion experiments, the Coulomb friction model tends to overestimate the friction stress, particularly under high contact pressures. When the friction stress is greater than the shear strength of the deformed material, shear flow stress should be used to replace the friction stress. Nevertheless, when the friction stress is lower than the shear strength of the deformed material, the friction stress should follow the Coulomb friction model. As a result, the combined friction model was selected in order to represent the tool-billet interface in this study.

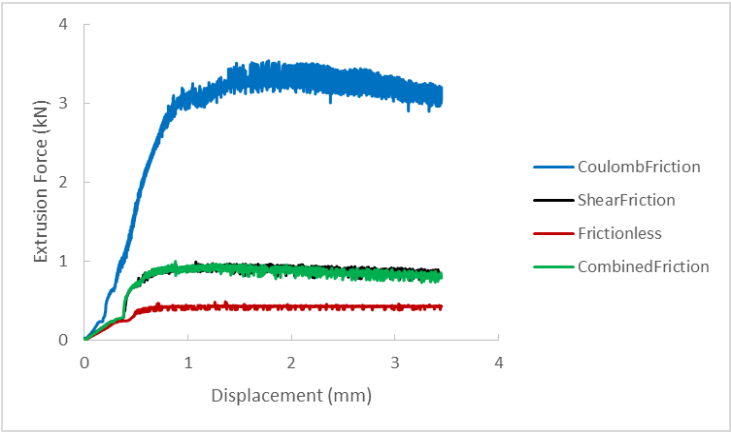

Fig. 6 Comparison of the friction models considered in this study.

Fig. 7 shows the micro-extrusion results comparison of between the experiment and simulation using combined friction model. Note that this experiment was carried out by using DLC-EX coating, which used the friction coefficient between tool-billet interface of 0.09. The error between the experimental and simulations results is approximately 4.7%. Thus, the combined friction model seems to be suitable for the micro-extrusion process.

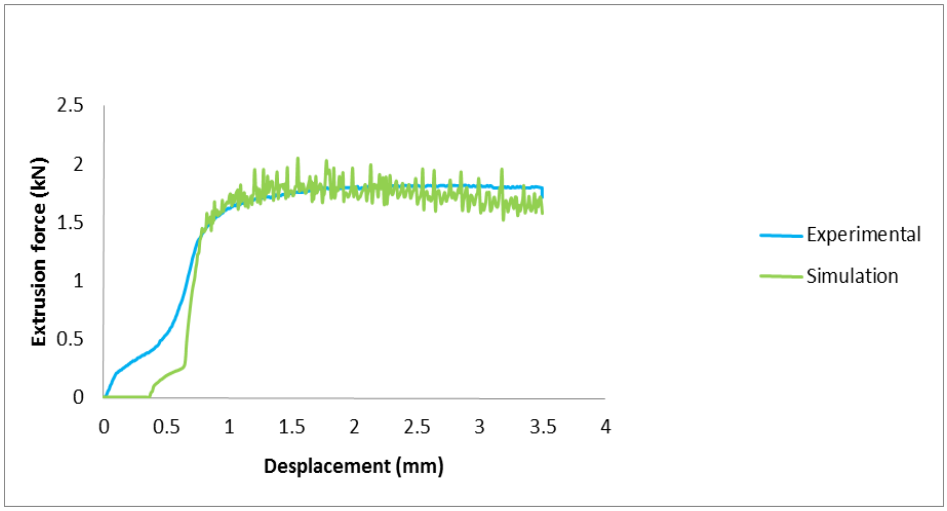

Fig. 7 Comparison results of the experiment and simulation using combined friction model.

The effects of tool geometry and position are illustrated in figures 8-11. It can be seen when the punch shift length (P_s) changes from 0 µm to 120 µm, no curving tendency of micro-extruded pins can be observed (Fig. 8). This shows that the slight change in punch position does not affect the material flow, which is being guided by the die geometry.

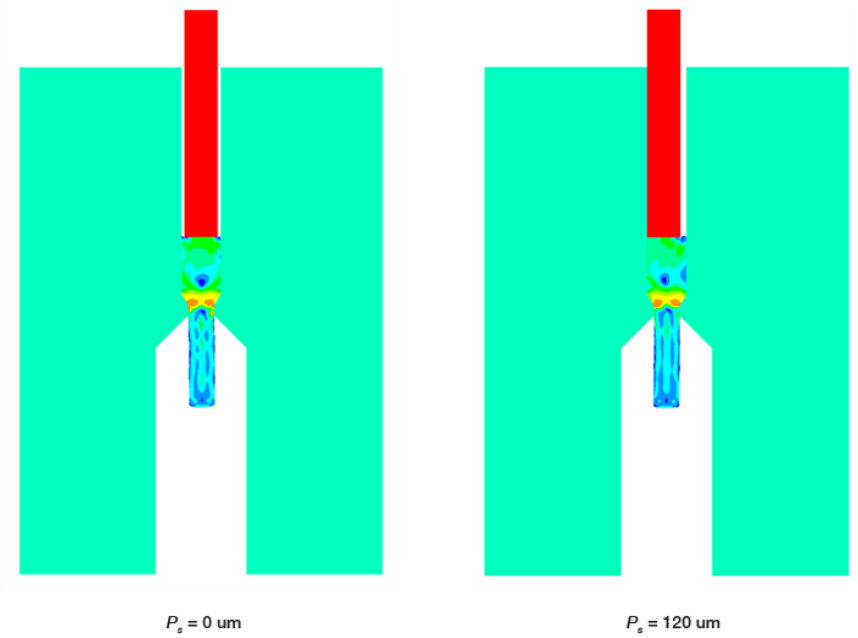

Fig. 8 FE results considering punch shift length (P_s)

Similarly, when die angle (α) changes from 30º to 60º to 90º, the curving tendency cannot be seen (Fig. 9). However, when the die shift length (D_s) varies from 0 µm to 100 µm, it can be seen that the micro-extruded pin is curved (Fig. 10). This is due to the fact that the one of the segmented dies is moved downward, causing the extruded billet to move against the exposed bearing area and curving to the extruded pin. In the experiment, if the segmented dies are not securely fixed, die shift can occur. If the bearing length (L_{br}) is increased from 0.5 mm to 1.0 mm while the die shift length (D_s) is 100 µm, the extruded pin changes from curve to straight. This is due to the fact that the increased bearing area helps control the straightness of the extruded pin. If the bearing length (L_{br}) is increased further from 1.0 mm to 1.5 mm, the extruded pin remain straight but the extrusion force is also higher. This is due to the increased bearing area, which generates higher friction between the tool-billet interface.

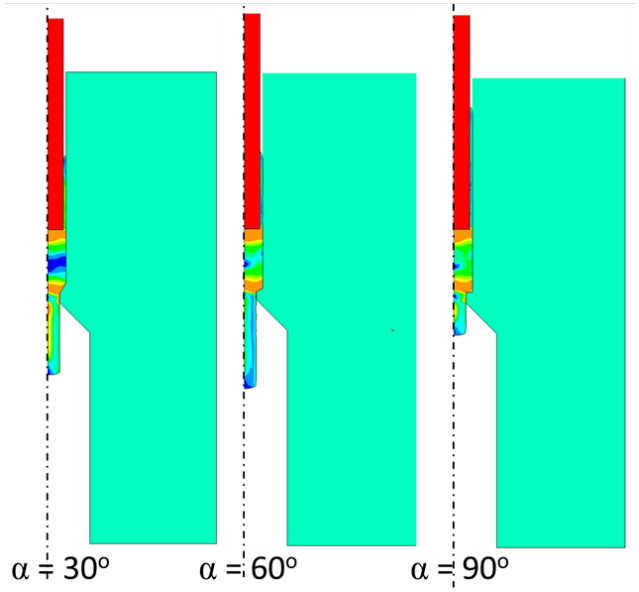

Fig. 9 FE results considering punch shift length (α)

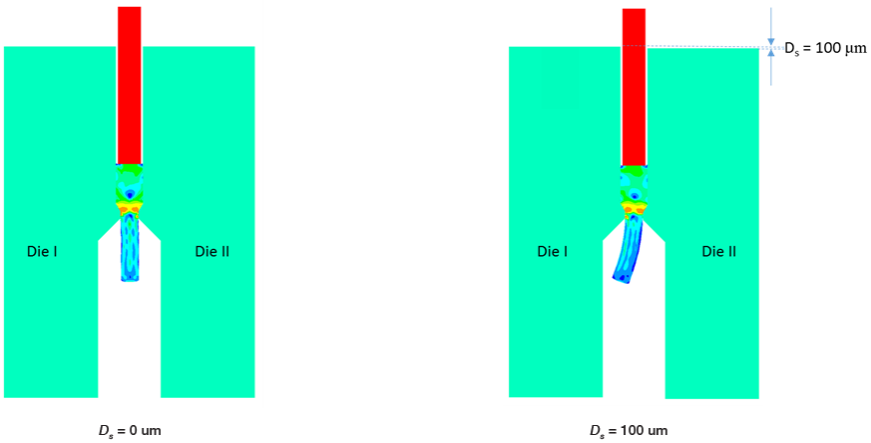

Fig. 10 FE results considering die shift length (D_s)

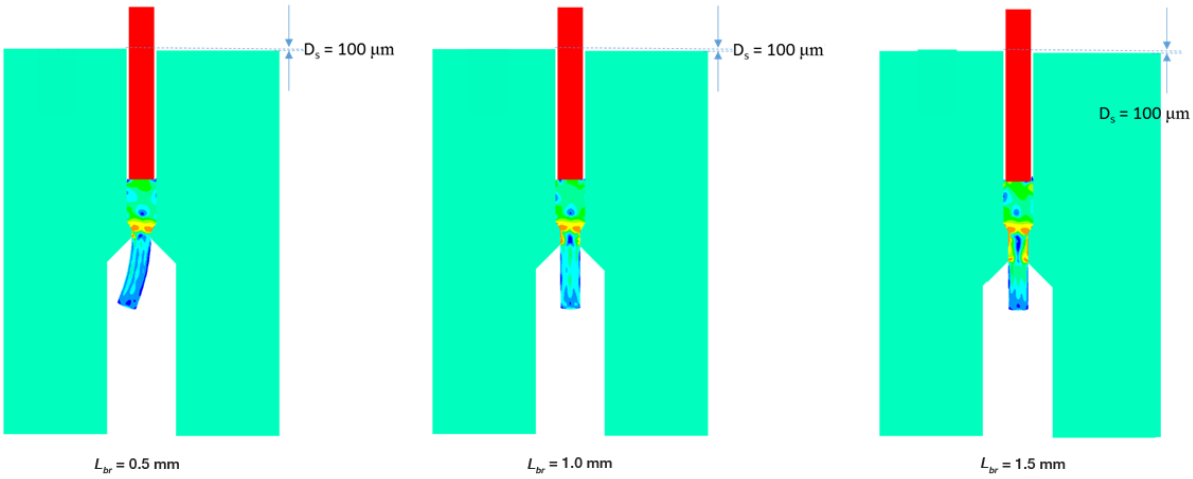

Fig. 11 FE results considering bearing length (L_{br})

Summary

This study investigated the effects of tool geometry and position on curving tendency in micro-extrusion of 6063 aluminum alloy. In order to select a suitable friction model for micro-extrusion, three friction models were considered: (1) Coulomb friction, (2) plastic shear friction, and (3) combined (Coulomb & plastic shear) friction. The results showed that the combined friction model should be applied in the micro-extrusion process. The finite element simulation of the micro-extrusion was carried out to investigate the effects of (1) punch shift length, (2) die angle, (3) die shift length, and (4) bearing length. Punch shift length and die angle did not affect the curving tendency of micro-extruded pins. Die shift length caused the micro-extruded pins to curve. The increased in bearing length helped straighten the curved pins.

Acknowledgement

The authors would like to acknowledge the supports of Thailand Research Fund under the grant number MRG5980148, National Metal and Materials Technology Center (MTEC), Thailand, University of Toyama, Japan, Department of Mechanical Engineering, Northwestern University, USA, and Department of Mechanical Engineering, Faculty of Engineering, Khon Kaen University, Thailand.

References

[1] Geiger, M., Kleiner, M., Eckstein, R., Tiesler, N., Engel, U., 2001. Microforming. CIRP Annals - Manufacturing Technology 50 (2), 445-462.
[2] Engel, U., Eckstein, R., Sep. 2002. Microforming—from basic research to its realization. Journal of Materials Processing Technology 125–126 (0), 35-44.
[3] Qin, Y., Jul. 2006. Micro-forming and miniature manufacturing systems — development needs and perspectives. Journal of Materials Processing Technology 177 (1–3), 8-18.
[4] Jeswiet, J., Geiger, M., Engel, U., Kleiner, M., Schikorra, M., Duflou, J., Neugebauer, R., Bariani, P., Bruschi, S., 2008. Metal forming progress since 2000. CIRP Journal of Manufacturing Science and Technology 1 (1), 2-17.
[5] Rosochowski, A., Presz, W., Olejnik, L., Richert, M., 2007. Micro-extrusion of ultra-fine grained aluminium 33 (1-2), 137-146+.

[6] Wang, C.-j., Guo, B., Shan, D.-b., Sun, L.-n., Sep. 2009. Effects of specimen size on flow stress of micro rod specimen. Transactions of Nonferrous Metals Society of China 19, Supplement 2, s511-s515.
[7] Chan, W. L., Fu, M. W., Yang, B., Aug. 2011. Study of size effect in micro-extrusion process of pure copper. Materials & Design 32 (7), 3772-3782.
[8] Deng, J. H., Fu, M. W., Chan, W. L., May 2011. Size effect on material surface deformation behavior in micro-forming process. Materials Science and Engineering: A 528 (13–14), 4799-4806.
[9] Parasız, S. A., Kinsey, B. L., Mahayatsanun, N., Cao, J., Aug. 2011. Effect of specimen size and grain size on deformation in microextrusion. Journal of Manufacturing Processes 13 (2), 153-159.
[10] Lin, J.-f., Li, F., Zhang, J.-f., Dec. 2012. A new approach to investigate real flow stress in micro extrusion. Transactions of Nonferrous Metals Society of China 22, Supplement 2, s232-s238.
[11] Ghassemali, E., Tan, M.-J., Wah, C. B., Jarfors, A. E. W., Lim, S. C. V., Oct. 2013. Grain size and workpiece dimension effects on material flow in an open-die micro-forging/extrusion process. Materials Science and Engineering: A 582, 379-388.
[12] Xinyun, W., Mao, Z., Na, T., Ning, L., Lin, L., Jianjun, L., 2013. A forming load prediction model in BMG micro backward extrusion process considering size effect. Physics Procedia 48 (0), 146-151.
[13] Ghassemali, E., Tan, M.-J., Jarfors, A. E. W., Lim, S. C. V., Jun. 2013. Optimization of axisymmetric open-die micro-forging/extrusion processes: An upper bound approach. International Journal of Mechanical Sciences 71, 58-67.
[14] Ghassemali, E., Tan, M.-J., Wah, C. B., Lim, S. C. V., Jarfors, A. E. W., Jan. 2015. Effect of cold-work on the Hall–Petch breakdown in copper based micro-components. Mechanics of Materials 80, Part A, 124-135.

Conference:	The 2017 World Congress on Micro and Nano Manufacturing (WCMNNM 2017)
Conference Location:	Taiwan
Paper Title:	Effect of Die Shift on Curvature of Micro-Extruded Pins
Proceeding Pages:	63-66

Effect of Die Shift to Curvature of Micro-Extruded Pins

WCMNM 2017 No.

Sedthawatt Sucharitpwatskul[1] Numpon Mahayotsanun[1] Sasawat Mahabunphachai[2] Norio Takatsuji[3] Kuniaki Dohda[4]

[1] Department of Mechanical Engineering, Faculty of Engineering, Khon Kaen University, Khon Kaen, 40002, Thailand
[2] National Metal and Materials Technology Center (MTEC), Thailand Science Park, Pathum Thani, 12120, Thailand
[3] Graduate School of Science and Engineering for Research, University of Toyama, Toyama, 930-8555, Japan
[4] Department of Mechanical Engineering, Northwestern University, Illinois, 60208 USA

Abstract

This paper investigated the effect of die shift to the bending tendency or curvature of micro-extruded pins by using finite element simulation. By considering the original die setup, the die shift lengths were varied from 0.0 mm 0.2 mm. In order to observe the effect of the die shift at higher lengths, the opening part of the die was cut open to leave room for the curvature of micro-extruded pins and the die shift lengths were extended up to 1.4 mm. After the micro-extrusion simulation, the curvature radii of the micro-extruded pins were measured. The results showed that the increased in die shift length led to the decrease in curvature radii of the micro-extruded pins. Particularly during the initial increase in die shift length, the curvature radii dramatically decreased. As a result, die shift should be avoided at the beginning of the micro-extrusion in order to reduce bending tendency of micro-extruded pins.

Keywords: Bending; Curvature; Die Shift; Finite Element Simulation; Micro-Extrusion.

1. Introduction

Micro-forming is one of the potential technologies to produce net-shape micro/meso parts [1-4] and micro-extrusion is one of the key processes in micro-forming. Micro-extrusion provides high production rates, is suitable for mass production, produces near-net-shape components, and allows for 3-dimensional part geometry. One of the most concerned problems in micro-extrusion is the curving tendency of micro-extruded pins. Several studies have been carried out to explain the curving tendency in micro-extrusion [5-14]. The main conclusion from these research works is that grain (crystal) orientations are the major driving force of curved pins if the grain size is large comparable to the specimen size. The authors of this paper are concerned if tool geometry and position could contribute to the curving tendency of the micro-extruded pins. As a result, this paper aims to investigate the effects of die shift on the curving tendency in micro-extrusion by using finite element (FE) simulation.

2. Method and Materials

2.1. Micro-Extrusion Experimental Setup

The forward-backward micro-extrusion was used in this study as shown in Fig.1. A set of conical segmented dies with die angle (α) of 30º had the container diameter of 1.71 mm and the bearing diameter of 1.09 mm. Chromium nitride (CrN) was coated on the die surface and the die had the average surface roughness (Ra) values of 0.05 µm. The diameter of the punch was 1.47 mm.

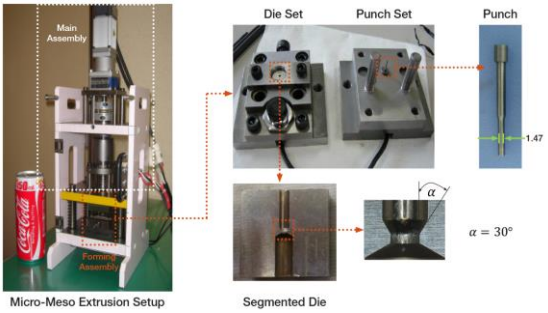

Fig. 1. Micro-extrusion experimental setup.

The material of both die and punch was SKD61. The test material under investigation was 6063 aluminum alloy. The specimen billets were fabricated to have 1.7 mm in diameter and 6 mm in length by hot extrusion and machining. The non-annealed billets had a microstructure having approximately 46 µm grain size and hardness value of 50 HV. The material model of the test material is expressed as in Eq. 1.

$$\sigma = (265.3\ \text{MPa})\ \varepsilon^{0.27} \quad (1)$$

where σ is flow stress and ε is strain. During the extrusion, test pieces (billets) were inserted into the die and pushed to form micro-extruded pin. The experiments were carried out at room temperature with a ram speed of 0.1 mm/s and a forming stroke of 3.5 mm.

2.2. Micro-Extrusion Finite Element Simulation

The numerical studies of the micro-extrusion were carried out in the Lagrangian finite element code MSC.Marc 2015. The micro-extrusion process was simplified with 2D axisymmetric analysis as shown in Fig. 2.

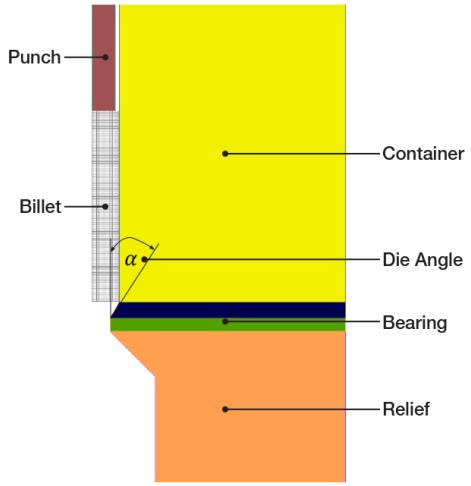

Fig. 2. Micro-extrusion simulation setup.

Note that the following assumptions were made: (1) 2D axisymmetric conditions, (2) no heat transfer to tools, and (3) using power law material model. Considering the symmetry of the process, an axisymmetric model was set up to simulate the extrusion process. The 4-node fully integration element was used. Totally, 2,040 elements were generated. The punch, container, die angle, bearing, and relief were designated as rigid bodies. The initial diameter of the cylinder billet was 1.7 mm and its height was 6 mm. The diameter of the formed part was 1.09 mm. The interface regions were 4 pairs, namely, punch-billet interface, container-billet interface, die angle-billet interface, and die bearing-billet interface. The combined friction model (Coulomb and shear friction models) was used. The coefficient of friction was 0.45 and the interface friction factor was 0.26. Note that the simulation results were compared with those of the experimental results by observing the extrusion force and stroke curves. The errors between the experimental and simulation results were within 4.7%, which was considered acceptable.

2.3. Die Shift Consideration

Since it was extremely difficult to control die shift in the experimental setup, finite element simulation was used to vary die shift lengths as demonstrated in Fig. 3. In this study, two die configurations were considered: (1) original die (with specific opening area at the outlet) and (2) opening die (with open outlet area for the micro-extruded pin to curve). The configurations of the both dies can be seen in Fig. 4. The die shift variation is shown in Table 1.

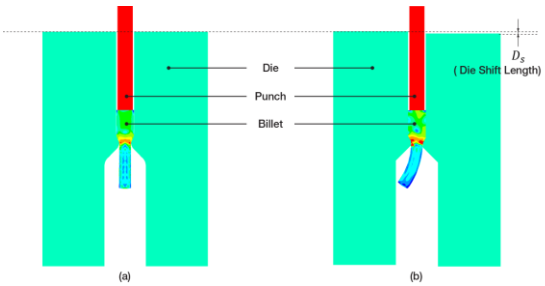

Fig. 3. Die shift configuration: (a) no die shift (D_s = 0 mm), and (b) die shift (D_s varies).

Table 1
Die shift variation considered in this study

Configuration	Die shift length (mm)
Original die	0.00, 0.05, 0.10, 0.20
Opening die	0.30, 0.40, 0.50, 0.60, 0.70, 0.80, 0.90, 1.00, 1.10, 1.20, 1.30, 1.40

2.3. Pin Curvature Radii Measurement

In order to observe the bending tendency of the micro-extruded pins, the pin curvature radii were measured after the finite element simulations were completed as shown in Fig. 4. Three curvature points were marked in the extruded pins in order to determine the curvature arc and center of the inner radius (R_{in}). Since the die shift created an outer pin distortion, the outer radius (R_{out}) of the pin was not uniformly extended from the inner radius. As a result, the outer radius was created and determine to match with the curvature of the pin. The average curvature radius (R_{avg}) could then be determined from the average of both inner radius and outer radius. Note that the values of R_{avg} of all the considered die shift variations were later used to compared and analysed.

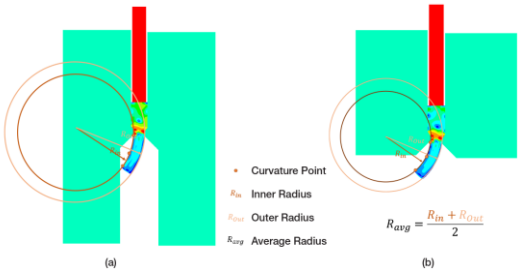

Fig. 4. Pin curvature radii measurement: (a) original die, and (b) opening die.

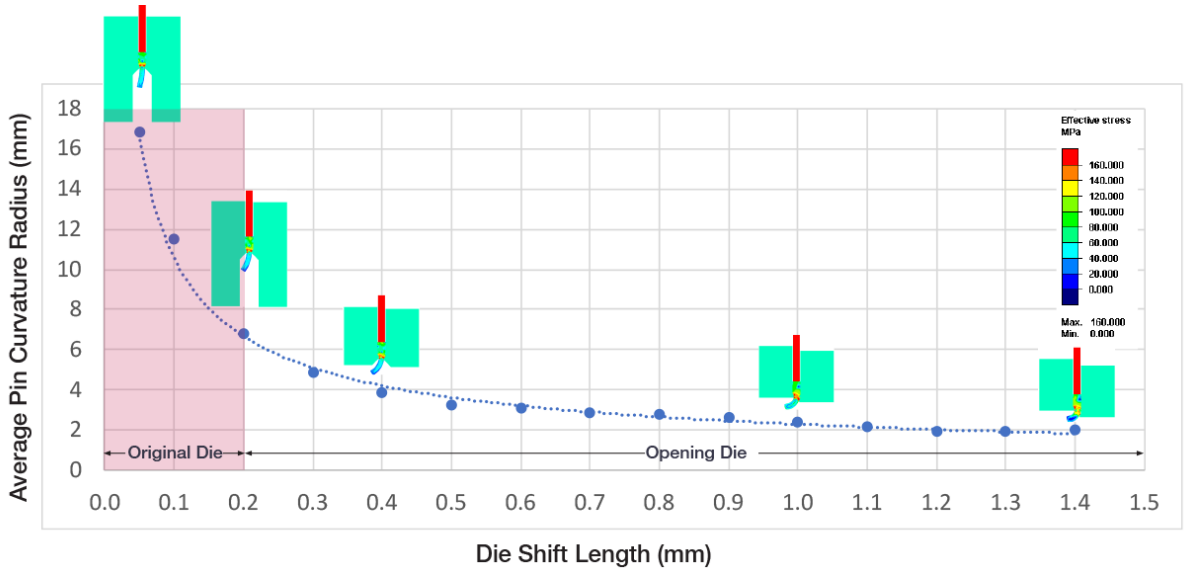

Fig. 5. Average pin curvature radius vs. die shift length.

3. Results and Discussions

Fig. 5 shows the average pin curvature radius plotted against die shift length. Note that both original die and opening die results were plotted on the same graph. It could be observed that the average pin curvature radii dramatically decreased with increasing die shift length for the original die. However, the average curvature radii gradually decreased with increasing die shift length for the opening die.

In other words, the initial die shift was the main cause for the micro-extruded pins to bend. As a result, it was crucially important to ensure the there was no die shift in order to avoid bending of micro-extruded pins.

4. Conclusions

The effect of die shift to bending tendency of micro-extruded pins was investigated by using finite element simulation. Two types of die were considered: (1) original die (with specific opening area) and (2) opening die (leaving open area for pins to curve). In the original die, the die shift lengths were increased from 0 mm to 0.2 mm and the simulation results showed that the curvature radii decreased dramatically with die shift lengths. In the opening die, the die shift lengths were increased from 0.3 mm to 1.4 mm. The simulation results showed that the curvature radii gradually decreased with increasing die shift lengths. The highlight of this paper demonstrated that initial die shift significantly contributed to the bending tendency of micro-extruded pins, which should be avoided.

Acknowledgements

The authors would like to acknowledge the supports of Thailand Research Fund under the grant number MRG5980148, National Metal and Materials Technology Center (MTEC), Thailand, University of Toyama, Japan, Department of Mechanical Engineering, Northwestern University, USA, and Department of Mechanical Engineering, Faculty of Engineering, Khon Kaen University, Thailand.

References

[1] Geiger, M., Kleiner, M., Eckstein, R., Tiesler, N., Engel, U., 2001. Microforming. CIRP Annals - Manufacturing Technology 50 (2), 445-462.
[2] Engel, U., Eckstein, R., Sep. 2002. Microforming—from basic research to its realization. Journal of Materials Processing Technology 125–126 (0), 35-44.
[3] Qin, Y., Jul. 2006. Micro-forming and miniature manufacturing systems — development needs and perspectives. Journal of Materials Processing Technology 177 (1–3), 8-18.
[4] Jeswiet, J., Geiger, M., Engel, U., Kleiner, M., Schikorra, M., Duflou, J., Neugebauer, R., Bariani, P., Bruschi, S., 2008. Metal forming progress since 2000. CIRP Journal of Manufacturing Science and Technology 1 (1), 2-17.
[5] Rosochowski, A., Presz, W., Olejnik, L., Richert, M., 2007. Micro-extrusion of ultra-fine grained aluminium 33 (1-2), 137-146+.
[6] Wang, C.-j., Guo, B., Shan, D.-b., Sun, L.-n., Sep. 2009. Effects of specimen size on flow stress of micro rod specimen. Transactions of Nonferrous Metals Society of China 19, Supplement 2, s511-s515.
[7] Chan, W. L., Fu, M. W., Yang, B., Aug. 2011. Study of size effect in micro-extrusion process of pure copper. Materials & Design 32 (7), 3772-3782.
[8] Deng, J. H., Fu, M. W., Chan, W. L., May 2011. Size effect on material surface deformation behavior in micro-forming process. Materials Science and Engineering: A 528 (13–14), 4799-4806.
[9] Parasız, S. A., Kinsey, B. L., Mahayatsanun, N., Cao, J., Aug. 2011. Effect of specimen size and grain size on deformation in microextrusion. Journal of Manufacturing Processes 13 (2), 153-159.
[10] Lin, J.-f., Li, F., Zhang, J.-f., Dec. 2012. A new approach to investigate real flow stress in micro extrusion. Transactions of Nonferrous Metals Society of China 22, Supplement 2, s232-s238.
[11] Ghassemali, E., Tan, M.-J., Wah, C. B., Jarfors, A. E. W., Lim, S. C. V., Oct. 2013. Grain size and

workpiece dimension effects on material flow in an open-die micro-forging/extrusion process. Materials Science and Engineering: A 582, 379-388.
[12] Xinyun, W., Mao, Z., Na, T., Ning, L., Lin, L., Jianjun, L., 2013. A forming load prediction model in BMG micro backward extrusion process considering size effect. Physics Procedia 48 (0), 146-151.
[13] Ghassemali, E., Tan, M.-J., Jarfors, A. E. W., Lim, S. C. V., Jun. 2013. Optimization of axisymmetric open-die micro-forging/extrusion processes: An upper bound approach. International Journal of Mechanical Sciences 71, 58-67.
[14] Ghassemali, E., Tan, M.-J., Wah, C. B., Lim, S. C. V., Jarfors, A. E. W., Jan. 2015. Effect of cold-work on the Hall–Petch breakdown in copper based micro-components. Mechanics of Materials 80, Part A, 124-135.